Science of Remote Sensing 8 (2023) 100110

Contents lists available at ScienceDirect

Science of Remote Sensing

journal homepage: www.sciencedirect.com/journal/science-of-remote-sensing

Modelling tree biomass using direct and additive methods with point cloud deep learning in a temperate mixed forest

Harry Seely [a,*], Nicholas C. Coops [a], Joanne C. White [b], David Montwé [a], Lukas Winiwarter [a,c], Ahmed Ragab [d,e]

[a] Integrated Remote Sensing Studio, Department of Forest Resource Management, University of British Columbia, 2424 Main Mall, Vancouver, BC, V6T 1Z4, Canada
[b] Canadian Forest Service (Pacific Forestry Centre), Natural Resources Canada, 506 West Burnside Road, Victoria, British Columbia, V8Z 1M5, Canada
[c] Research Unit Photogrammetry, Department of Geodesy and Geoinformation, TU Wien, Wiedner Hauptstraße 8-10, 1040, Vienna, Austria
[d] CanmetENERGY, Natural Resources Canada, 1615 Lionel-Boulet Blvd, P.O. Box 4800, Varennes, Québec, J3X 1P7, Canada
[e] Department of Mathematics and Industrial Engineering, Polytechnique Montreal, Québec, H3T 1J4, Canada

ARTICLE INFO

Keywords:
Deep neural network (DNN)
Airborne laser scanning (ALS)
Tree component biomass
DGCNN
Octree-CNN (OCNN)
Model comparison

ABSTRACT

Airborne laser scanning (ALS) data has been widely used for total aboveground tree biomass (AGB) modelling, however, there is less research focusing on estimating specific tree biomass components (wood, branches, bark, and foliage). Knowledge about these biomass components is essential for carbon accounting, understanding forest nutrient cycling, and other applications. In this study, we compare additive AGB estimation (sum of estimated components) with direct AGB estimation using deep neural network (DNN) and random forest (RF) models. We utilise two point cloud DNNs: point-based Dynamic Graph Convolutional Neural Network (DGCNN) and Octree-based Convolutional Neural Network (OCNN). DNN and RF models were trained using a dataset comprised of 2336 sample plots from a mixed temperate forest in New Brunswick, Canada. Results indicate that additive AGB models perform similarly to direct models in terms of coefficient of determination (R^2) and root-mean square error (RMSE), and reduced the mean absolute percentage error (MAPE) by 22% on average. Compared to RF, the DNNs provided a small improvement in performance, with OCNN explaining 5% more variation in the data ($R^2 = 0.76$) and reducing MAPE by 20% on average. Overall, this study showcases the effectiveness of additive tree AGB models and highlights the potential of DNNs for enhanced AGB estimation. To further improve DNN performance, we recommend using larger training datasets, implementing hyperparameter optimization, and incorporating additional data such as multispectral imagery.

1. Introduction

Forest biomass stores approximately 861 billion metric tons of carbon globally, amounting to 50–65% of all terrestrial carbon (Pan et al., 2011; Reichstein and Carvalhais, 2019). As such, modelling tree biomass is critical for improving our understanding of the terrestrial carbon cycle, and assessing the effects of climate change on forest biomes. Accurate estimation of tree biomass is vital for sustainable forest management and is required for a variety of applications such as mapping forest fuels. Tree biomass modelling is also becoming increasingly important worldwide with the rise of carbon credit systems (Duncanson et al., 2019; Kumar et al., 2021).

To date, most of the research focused on estimating tree biomass has implemented models that estimate the total aboveground biomass (AGB) of trees. However, in many situations, estimates of total AGB are insufficient, and specific knowledge about the components of tree biomass is necessary (Magalhães and Seifert, 2015). For example, total AGB is too broad of a carbon pool to be used in many terrestrial carbon cycle models that require more specific allocation to carbon pools (e.g., foliage) as inputs (Bloom et al., 2016). In addition, the quantification of unmerchantable tree biomass components is necessary in situations where biomass components are targeted for use as bioenergy, fiber, or other purposes (Peter and Niquidet, 2016; Turrado Fernández et al., 2016).

Generally, tree AGB is partitioned into four distinct components: wood (i.e., stem), branches, bark, and foliage (Sanquetta et al., 2015). A common method for estimating tree biomass components is to fit separate models for each component in addition to a total AGB model (e.g.,

* Corresponding author.
E-mail address: hseely@student.ubc.ca (H. Seely).

https://doi.org/10.1016/j.srs.2023.100110
Received 4 August 2023; Received in revised form 11 November 2023; Accepted 14 November 2023
Available online 18 November 2023

Popescu, 2007). However, this approach implies that component estimates are not relative, and do not necessarily sum to equal the estimated total AGB. In contrast, an additive approach to AGB estimation involves modelling biomass components simultaneously in a single model and then summing the components to get total AGB. The additive approach is useful in biomass components modelling because it ensures: 1) relative estimation of biomass components; and 2) that the sum of component biomass equals total AGB (Affleck and Diéguez-Aranda, 2016; Parresol, 2001; Zhao et al., 2019). The use of additive biomass equations is also a common practice when deriving individual tree biomass estimates in the field (Lambert et al., 2005; Ung et al., 2008).

There are several other reasons why estimating biomass components is beneficial. Component-based biomass estimation is essential for many ecological applications, such as forest nutrient cycling (Rodríguez-Soalleiro et al., 2018) and evaluating plant productivity (Benomar et al., 2012). It is also crucial for achieving precise forest carbon models as different components typically have different carbon concentrations (Rodríguez-Soalleiro et al., 2018). Many carbon models assume that 50% of tree biomass is carbon; however, several studies have demonstrated that the carbon concentration can vary between components depending on species, age, diameter at breast height (DBH), site conditions and other factors (Dong et al., 2016; Rodríguez-Soalleiro et al., 2018; Widagdo et al., 2020). Similarly, the duration of time that carbon remains in a specific component can vary (Zhang et al., 2010). Lastly, many large-scale carbon models, such as the Carbon Budget Model of the Canadian Forest Sector (CBM-CFS3), use information regarding carbon estimates by tree component (Kurz et al., 2009; Natural Resources Canada, 2022).

When a model is developed for direct AGB estimation, it is optimized to estimate a single value. In contrast, estimating tree biomass components through multi-output regression becomes a more challenging task as it must balance multiple objectives. Ayrey et al. (2021) highlighted this challenge when estimating multiple forest attributes (e.g., AGB, tree count, species composition, etc.) within a single model. However, it should be noted that modelling the biomass of tree components is likely more feasible compared to the different types of variables (e.g., volume, count, proportion) targeted by Ayrey et al. (2021). As such, it is worth investigating whether additive tree biomass models are as effective as models that are optimized to directly estimate AGB.

Over the past two decades, lidar has proven to be useful for estimating tree AGB due to its ability to measure three-dimensional (3D) forest structure. Unlike passive optical approaches (such as photogrammetry), lidar can penetrate gaps in the tree canopy to capture a detailed representation of the forest's vertical structure (Nguyen et al., 2018; White et al., 2016). A variety of lidar systems have been applied for AGB estimation, with airborne laser scanning (ALS) being the most prevalent (Kristensen et al., 2015; Zhao et al., 2009). There are also a growing number of studies implementing terrestrial laser scanning (TLS) (e.g., Momo Takoudjou et al., 2018), and spaceborne systems such as ICESat and GEDI (e.g., Duncanson et al., 2020; Narine et al., 2019; Shendryk, 2022), among other lidar systems such as backpack laser scanning (Xu et al., 2021).

The most common workflow for estimating tree AGB with ALS data involves using allometry-derived biomass estimates in ground reference plots to develop a model with co-located, area-based lidar metrics (i.e., statistics summarizing lidar returns). For example, McRoberts et al. (2015) estimated forest AGB across 825 ha of Norwegian coniferous stands using 20 ALS height metrics in an ordinary least squares (OLS) model, achieving R^2 values between 0.69 and 0.91. A similar approach in Finland developed nationwide OLS biomass models using two lidar metrics as predictors, and achieved a relative Root Mean Square Error (rRMSE) between 20% and 25% (Kotivuori et al., 2016). Other research has leveraged lidar metrics to estimate tree AGB using more advanced Machine Learning (ML) frameworks such as K-Nearest Neighbor (KNN), Random Forest (RF) and Support Vector Regression (SVR) (Cosenza et al., 2021; Navarrete-Poyatos et al., 2019; Rex et al., 2020). For example, Cosenza et al. (2021) compared OLS, KNN and RF biomass models using ALS metrics across study sites in Brazil, Finland, Norway, and the USA. The results showed that both RF and OLS were effective (R^2 between 0.89 and 0.96), whereas the KNN was less accurate due to overfitting. Overall, the relative performance of a specific lidar biomass model appears to be dependent on the forest type and input data characteristics (e.g., sensor type, spatial error) for a given study. However, more complex ML models often outperform their simpler OLS counterparts (Ayrey and Hayes, 2018; Zhang et al., 2022; Zolkos et al., 2013).

Compared to total AGB estimation, there are fewer studies that apply lidar to estimate tree component biomass. Early research used lidar-derived individual tree DBH estimates in generalized allometric equations to estimate tree component biomass in small stands (e.g., Popescu, 2007). While this approach was effective for modelling tree component biomass in a monoculture plantation, it did not transfer well to complex stands (Xu et al., 2021). More recently, different approaches have been applied for lidar-based tree component biomass estimation, using individual tree- and area-based methods (Tsitsi, 2016; Xu et al., 2021). For example, García et al. (2010) used lidar height and intensity metrics in an OLS model to estimate foliage and branch biomass at the plot scale in a mixed stand, achieving R^2 values of 0.58 for foliage and 0.67 for branches. A subsequent study by Kankare et al. (2015) used ALS metrics in an RF model to predict tree component biomass, achieving rRMSEs of 26.7%, 32.6% and 49.6%, for stem, canopy and branches, respectively. Domingo et al. (2019) estimated forest residual biomass (FRB; sum of foliage, branches, and stem tops) in a managed stand using SVR, RF and multiple linear regression (MLR), and other decision tree models with height metrics derived from ALS data and achieved an R^2 between 0.77 and 0.82 and an rRMSE between 26.4% and 30.4%. In general, studies modelling tree component biomass using ALS metrics have been limited to smaller datasets (e.g., 45–226 plots) and attain lower accuracy compared to studies modelling total AGB. Moreover, many studies develop separate models for biomass components that do not preserve inter-component relationships or maintain additivity (e.g., García et al., 2010; Popescu, 2007).

Deep learning (DL) is a type of ML that has increased in prominence as a result of its predictive accuracy and capacity to harness big data (Ma et al., 2019; Zhang et al., 2016). Deep learning models, also referred to as Deep Neural Networks (DNNs), can learn abstract features from input data using several layers of interconnected "neurons" (mathematical models of brain neurons; LeCun et al., 2015). These learned features are numerical representations of the original input data that guide the DNN towards making a prediction. Since the development of the benchmark Convolutional Neural Network (CNN) called AlexNet in 2012 (Krizhevsky et al., 2012), DNNs have rapidly become widespread in the fields of forestry and remote sensing (RS) (Hamedianfar et al., 2022; Ma et al., 2019). DNNs have been adopted for several reasons, including their capacity to capture complex nonlinear interactions between input variables and their ability to learn nuanced patterns in large datasets (LeCun et al., 2015). There is a growing body of evidence that DNNs outperform conventional ML models across a variety of tasks, including tree segmentation (Weinstein et al., 2020), species identification (Mäyrä et al., 2021), and multi-output forest attribute regression (Ayrey et al., 2021).

Unlike conventional ML models where input features (e.g., ALS metrics) must be selected by a human based on expert-knowledge or through feature selection algorithms (e.g., Boruta; Kursa and Rudnicki, 2010), DNNs can learn features directly from the raw data (e.g., the ALS point cloud). This aspect of deep learning removes a degree of modeler bias and uncertainty in metric selection (Ayrey and Hayes, 2018). In the case of ALS modelling, DNNs are useful because they do not require dimensionality or resolution adjustment typically required for engineered input features. Since machine learning models tend to perform better given larger and more diverse datasets (Jang and Cho, 2019), it has been hypothesized that using the original lidar point cloud as input in a DNN, rather than lidar metrics, will result in improved tree biomass

predictive accuracy (Ayrey et al., 2021; Ayrey and Hayes, 2018; Oehmcke et al., 2022).

Despite the emerging potential of DNNs, applying these models to estimate tree biomass directly from ALS point clouds is challenging. Point clouds are unordered, unstructured, and irregular datasets. This means that conventional CNNs which require ordered data without sparsity are unsuitable for point cloud data (Bello et al., 2020; Qi et al., 2017a). Recently, a growing body of DL research has addressed these challenges using DNN architectures that can learn from a point cloud or similar 3D representation (e.g., voxel, octree). DNN architecture refers to the design and arrangement of the model, including several hyperparameters such as the number of layers, the number of neurons in each layer, and the mathematical operations connecting neurons. A DNN architecture is dependent on the structure of the input data, the desired model output, and the learning mechanisms implement in the model (e.g., convolutions). Architecture is thus an important determinant for the performance of a given DNN (Alzubaidi et al., 2021).

In the case of point cloud DNNs, there are three broad types of architectures (Bello et al., 2020; Zhao et al., 2021), all of which have been applied for forest attribute modelling: projection/view-based, voxel/octree-based, and point-based. Projection- and view-based point cloud DNNs use an approach where the point cloud is converted into 2D rasters viewed from potentially multiple perspectives, which are then fed through 2D CNNs (e.g., Briechle et al., 2021). Voxel- and octree-based models convert the point cloud into an ordered format, and then perform 3D convolutions on the reformatted data. Point-based DNNs learn directly from the point cloud using a combination of techniques such as multi-layered perceptrons (MLPs), point downsampling, and graph representation (e.g., Liu et al., 2022b). Depending on the dataset and modelling task, some types of point cloud DNNs perform better than others. As such, a comparison of different point cloud DNN architectures is beneficial for new applications such as biomass modelling.

Recently, point cloud DNNs have been applied instead of conventional OLS and ML lidar metric models to estimate forest AGB. For example, a study conducted by Ayrey and Hayes (2018) tested five voxel-based 3D CNNs to estimate plot-level tree AGB in the New England Acadian forest. In a similar vein, Oehmcke et al. (2022) modeled tree AGB in Denmark using the point-based DNNs PointNet and KPConv in addition to the voxel-based Minkowski Network. Both studies observed that point cloud DNNs outperformed conventional ML models (e.g., RF), reducing RMSE by up to 17% compared to their simpler ML and OLS counterparts. The early success of modelling total tree AGB using point cloud deep learning suggests that tree component biomass estimation could also be improved using similar methods.

The objective of this study is to compare the application of conventional ML and point cloud DNNs for additive and direct tree AGB regression. Specifically, this study will explore two research questions:

1. How does estimating total tree AGB through biomass components using an additive approach compare to estimating total AGB directly?
2. How do point cloud DNNs compare to conventional ML in terms of tree biomass estimation accuracy?

2. Methods

2.1. Study area

The province of New Brunswick in Canada was selected as the study area due to the availability of wall-to-wall ALS coverage (GeoNB, 2022) and a large network of forest sample plots (Fig. 1). New Brunswick is located along the coast in Eastern Canada and covers an area of approximately 72,908 km^2. The province has an average temperature of 11 °C and has 1110 mm of annual precipitation. The forests of New Brunswick cover approximately 85% of the province (6.1 million hectares) and are divided between public and private ownership (Martin, 2003). Roughly half the provincial forests are government crownland, with the remaining managed as private woodlots (29%) and industrial freehold (18%) (Martin, 2003). New Brunswick forests are characterized by a mixture of tree species resulting from a transition between the maritime broadleaf forests to the South and the boreal coniferous forests to the North (Martin, 2003; Zelazny et al., 2007). Dominant broadleaf species in the province include birch and maple, and dominant conifers

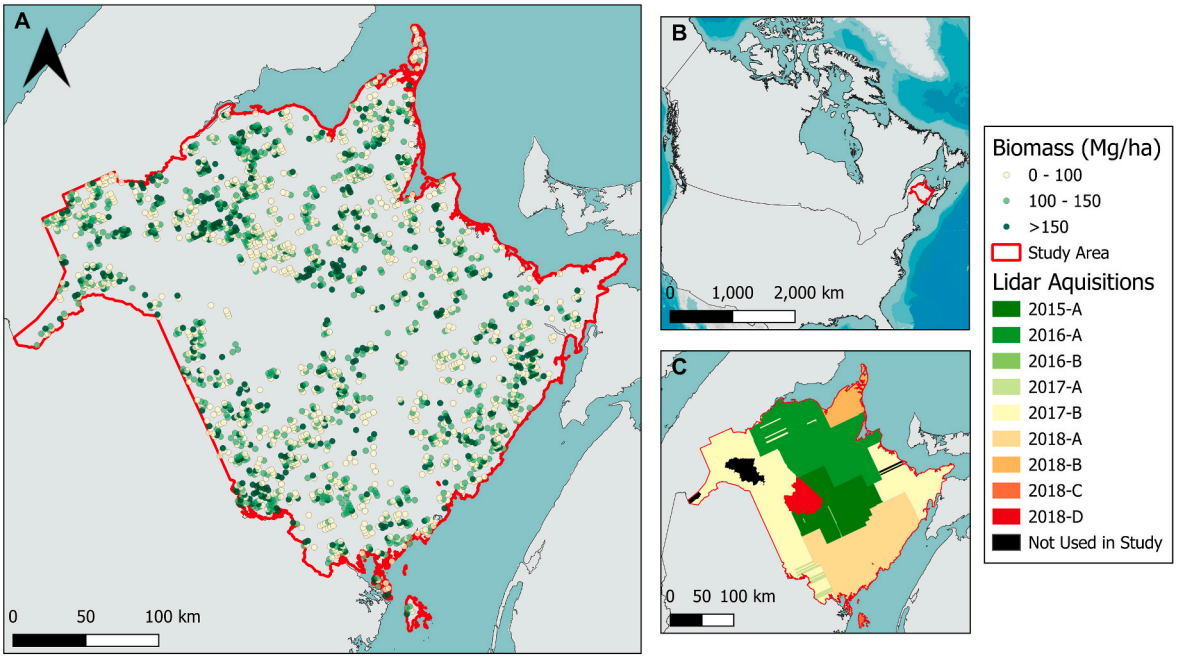

Fig. 1. Map of Continuous Landscape Inventory (CLI) plots in Province of New Brunswick (study area) in Canada. Panel A shows aboveground biomass (AGB) in metric tons per hectare (Mg/ha) for each ground plot. Note that only CLI plots which met the criteria described in the text are shown. Panel B shows the location of the study area in North America. Panel C shows the lidar acquisitions used in this study, which are summarized in more detail in Table 1.

include fir and spruce. The forests of New Brunswick are some of the most productive in Canada with an estimated mean net primary productivity of 302 g C/m^2 annually (Liu et al., 2002). New Brunswick forests have a relatively balanced age distribution with a mean age of 66 years and old forest (>150 years) comprising <5% of the forested area (Maltman et al., 2023).

2.2. Field data

Ground plot data from New Brunswick used in this study comes from the Continuous Landscape Inventory (CLI) dataset, which includes sample plots located on a fixed 2 × 2 kilometer grid spanning the province. Ground plots were primarily sampled in 2017 and 2018 between May and September. Plot centre coordinates were collected using survey grade GPS, generally providing a spatial error margin <25 cm. While there are over 7000 plots in the CLI dataset, only a subset of samples from the plot network were selected for use in this study. Based on the recommendations for handling forest plot outliers described in Knott et al. (2023), four criteria were implemented in this study to ensure accurate ground reference plots: 1) complete spatial overlap with lidar data; 2) field sampling within ± 3 years of lidar acquisition; 3) 95th height percentile in plot is greater than 1.5 m (i.e., significant tree biomass is present); and 4) an absolute difference of less than 3 m between ground-estimated Lorey's height (average height of all trees in a stand weighted by tree basal area) and the 95th height percentile measured by lidar. A total of 2336 plots met these criteria. Each CLI plot had a 11.28 m radius (400 m^2 plot area). For trees within a plot with DBH≥7.1 cm and small trees (DBH≥1 cm) in the inner 4 m radius of the plot, DBH, species, and health (alive vs. dead) were recorded. In each plot, a prism-sweep with a Basal Area Factor (BAF) of 2 was performed, and the height of every 10th sample tree was measured with a hypsometer, and subsequently used to calculate plot-level Lorey's height.

2.3. Lidar data

This study uses the publicly available ALS data spanning New Brunswick (GeoNB, 2022). Table 1 summarizes the ALS data collected over the course of nine different acquisitions from 2015 to 2018 between the months of June and October. ALS point density ranged from 13 to 31 points/m^2, with an average density of 21 points/m^2. Flight characteristics varied between acquisitions, including a flying height ranging from 1000 m–1200 m, horizontal accuracy between 0.20 m–0.31 m, and vegetated vertical accuracy between 0.07 m–0.59 m. The scan angles were between −40° and 38° off-nadir.

Table 1
Lidar acquisition information for the ALS data used in this study.

Name	Start Date	End Date	Mean Point Density (pts/m^2)	Number of Plots	Horizontal Accuracy (m)	Vegetated Vertical Accuracy (m)
2015-A	2015-08-02	2015-09-28	15.19	186	0.26	0.28
2016-A	2016-06-17	2016-10-04	19.50	675	NA	0.12
2016-B	2016-06-24	2016-06-24	13.18	4	0.31	0.28
2017-A	2017-06-12	2018-06-23	23.12	22	0.30	0.59
2017-B	2017-07-06	2017-08-16	19.39	791	0.30	0.39
2018-A	2018-06-11	2018-08-25	23.23	536	0.20	0.33
2018-B	2018-07-11	2018-08-11	29.39	129	0.20	0.07
2018-C	2018-07-30	2018-08-24	17.46	6	0.20	0.27
2018-D	2018-07-31	2018-08-31	31.77	1	0.20	0.23

The preprocessing steps for lidar point clouds included filtering duplicate points, creating a digital terrain model, and performing height normalization. Outlier points were classified and removed using the Statistical Outlier Removal (SOR) function with 9 neighbors and a distance multiplier of 3 (Rusu and Cousins, 2011). While many studies using lidar data for biomass estimation remove ground returns, recent research by Mahoney et al. (2022) demonstrated that ground point inclusion can improve ALS biomass model performance. As such, ground points were included in the analysis. All lidar pre-processing was performed using the lidR package (v. 4.0.1; Roussel et al., 2020) in R Software (v. 4.2.2; R Core Team, 2023).

2.4. Deriving reference component biomass

The Canadian national biomass equations developed by Lambert et al. (2005) and Ung et al. (2008) were applied to the ground reference data to estimate tree component biomass. These equations were developed for 24 common Canadian tree species using 9209 destructively sampled trees from across Canada. Unlike some allometric equations which are generalized, these equations are species-specific. Equations (1)–(4) show how DBH is used to estimate tree component biomass (y), where the parameters (β_1 and β_2) and error (e) differ depending on the tree species. Equation (5) shows how all biomass components (wood, bark, branches, and foliage) for a tree sum to derive the tree total AGB (y_{total}). Plot total AGB in tons (Mg) is derived by summing y_{total} for all trees in a plot, and is converted to a tons per hectare value (Mg/ha). For trees in the dataset that did not have a matching allometric equation (4% of all trees in ground data), equation parameters of a similar surrogate species were substituted. Fig. 1 shows the distribution of ground plots across New Brunswick coloured by total AGB in tons per hectare.

$$y_{wood} = \beta_{wood1} DBH^{\beta_{wood2}} + e_{wood} \quad \text{Equation 1}$$

$$y_{bark} = \beta_{bark1} DBH^{\beta_{bark2}} + e_{bark} \quad \text{Equation 2}$$

$$y_{branches} = \beta_{branches1} DBH^{\beta_{branches2}} + e_{branches} \quad \text{Equation 3}$$

$$y_{foliage} = \beta_{foliage1} DBH^{\beta_{foliage2}} + e_{foliage} \quad \text{Equation 4}$$

$$y_{total} = y_{wood} + y_{bark} + y_{branches} + y_{foliage} \quad \text{Equation 5}$$

2.5. Preparing data for machine learning

DNNs are sensitive to large variations in magnitude for both input and target variables (Krizhevsky et al., 2012). Tree component biomass values can vary substantially in magnitude, as values of wood and branch biomass are typically much larger relative to bark and foliage. In the New Brunswick plot dataset, the majority of total tree AGB is wood (66%) with the remaining components comprising smaller proportions (14% branch, 10% bark, 10% foliage). To account for the imbalance in component biomass, following the methods of Ayrey et al. (2021), target biomass values were normalized to Z-score values using the mean and standard deviation of the plot level values for each component. Z-score normalizing ensures that all biomass components contribute the same magnitude of error to avoid biasing the model towards components with greater biomass. For direct AGB models, Z-score normalization was not implemented as it did not improve model performance in early experiments. The XYZ coordinates of each input point cloud were reduced by subtracting the mean from each coordinate value following the approach of Winiwarter et al. (2019). This subtraction centered the point cloud around the origin, aligning its centroid with (0, 0, 0) in the XYZ space. The reduction of coordinates ensures a consistent value range across all sample point clouds, thus preventing large values from influencing neuron weights. Lidar intensity values were rescaled using max-min normalization for each plot separately. Other lidar attributes

including classification, scan angle, return number, and number of returns were not rescaled as they fell within the same value range as the coordinates and intensity. Finally, plots were split into train (70%, n = 1635), validation (15%, n = 350), and test (15%, n = 351) sets using random sampling. Since individual plots are spatially separated by > 2 km, a spatial split was not deemed necessary.

Data augmentation is a common preprocessing step in DL where distortions, noise addition, and other modifications are made to predictor variables in the train set to increase input data diversity and reduce overfitting (Oubara et al., 2022). Importantly, data augmentation is only applied to the predictor variables (point clouds), not the target variables (reference biomass values). Data augmentation was applied to the training point clouds in the form of random rotation around the Z-axis, random noise addition to individual points (i.e., jittering), and shifting all points by a randomly chosen distance along each axis. For the DNNs, training data was augmented on-the-fly through rotation, jittering, and shifting prior to each epoch during training (Qi et al., 2017a). For RF, the same data augmentation was treated as a hyperparameter and was implemented prior to lidar metric calculation.

Fig. 2 compares the three modelling pathways we used to estimate tree biomass in this study: conventional ML using random forest, octree-based DNN, and point-based DNN. The three following sections describe the details of how these models were applied, including information regarding input data structure and the learning mechanism.

2.6. Conventional machine learning approach

Random forest (RF) represents a conventional ML approach commonly used in conjunction with lidar metrics for tree biomass estimation (Ayrey and Hayes, 2018; Kanmegne Tamga et al., 2023; Zhou et al., 2022). RF often outperforms other ML models such as KNN and SVR and is widely used in remote sensing research (Belgiu and Drăguţ, 2016). The major strength of RF is its nature as an ensemble model through the generation of many classification and regression trees (CARTs), each of which casts a vote contributing to the final prediction (Breiman, 2001). RF models have many benefits, such as the capacity to handle high dimensionality data, in addition to being robust towards multicollinearity and overfitting (Belgiu and Drăguţ, 2016). RF was implemented in this study using the Scikit-Learn package (v. 1.3.0; Pedregosa et al., 2011) with Python version 3.8.

RF models were trained with plot-level lidar metrics summarized in a tabular format. A suite of 86 lidar metrics were selected as candidate predictors in the RF model based on their use in previous forest attribute modelling (e.g., White et al., 2015; Woods et al., 2008; Xu et al., 2019). These included common height statistics (e.g., height percentiles), vegetation metrics (e.g., leaf area density) and canopy metrics (e.g., canopy relief ratio). A full list of lidar metrics used in this study is available in Appendix A. Lidar metrics were calculated using the pyForMetrix Python package (v. 0.0.6; Winiwarter, 2023), which is an adaptation of the lidRmetrics package (Tompalski et al., 2023). Variable selection was performed based on the methods of Ayrey and Hayes

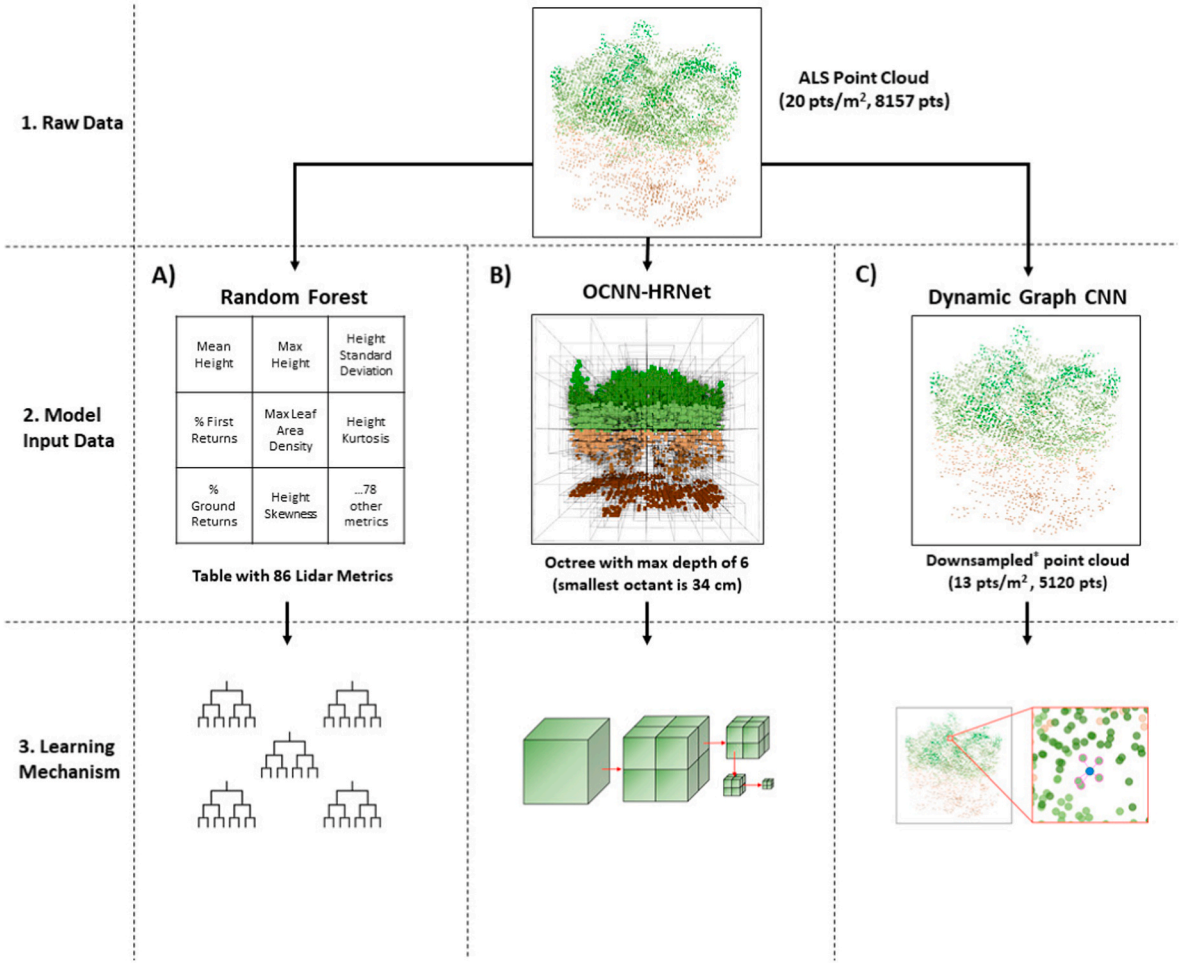

Fig. 2. Comparing the raw data, model input, and learning mechanisms for random forest (RF), Octree CNN (OCNN) HRNet and Dynamic Graph CNN (DGCNN) models. Visual representation for OCNN and DGCNN are adapted from Wang et al. (2017, 2019), respectively. *The downsampled point cloud shown was derived using random sampling.

(2018), where after an initial run of RF using all variables, those with an importance score below a threshold (treated as a hyperparameter) were dropped. Fig. 2A summarizes the RF model workflow used in this study including the input data format and learning mechanism.

2.7. Octree-based deep neural network

Octree-CNNs (OCNNs) have been demonstrated across several studies to be simple, efficient, and effective approaches to point cloud deep learning (Wang et al., 2017, 2018, 2020, 2021). OCNNs operate similarly to voxel based networks such as the Minkowski Engine (Choy et al., 2019) and SparseConvNet (Schmohl and Sörgel, 2019), but are typically faster and more memory-efficient. OCNNs adapt conventional CNN model architectures (e.g., LeNet) to perform 3D convolutions on an octree representation of a point cloud (Wang et al., 2017). High-Resolution Net, or HRNet, (Sun et al., 2019) is an established CNN commonly used in image analysis for a variety of tasks such as segmentation (Zhang et al., 2020) and classification (Xu et al., 2022). As such, the HRNet-OCNN model architecture developed by Wang et al. (2021) was selected for this study and applied using the OCNN-Pytorch Python package (Wang, 2023).

As shown in Fig. 2B, converting a lidar point cloud into an octree structure means recursively subdividing the point cloud into 8 child cubes (octants) until the maximum octree depth is reached. In this study, a max octree depth of 6 was used, meaning that due to variation in point cloud height, the smallest octant (i.e., cube) ranged between 33 cm and 50 cm and was 34 cm on average. Each octant had associated XYZ coordinates, intensity, classification, return number, number of returns, scan angle, and estimated XYZ components of the surface normal (i.e., the directional vector on the point cloud surface). Surface normals were estimated using the Open3D Python package (v. 0.17.0) through the KD Tree Search KNN algorithm with a max nearest neighbor value of 30 (Zhou et al., 2018). In cases where multiple points lay within an octant, the average value was taken for each lidar attribute. Empty octants were labelled as zero across all attributes. OCNN-HRNet learns multi-resolution features by performing 3D convolutions on each octree depth along parallel subnetworks (Fig. 2B; Wang et al., 2021). Batch normalization is implemented throughout the network, and learned features are aggerated through mean and max pooling operations. A fully-connected (FC) module at the back-end of the network provides a final predicted biomass value.

2.8. Point-based deep neural network

A variety of point-based DNN architectures have been applied for forest attribute modelling in prior research (e.g., Hell et al., 2022; Liu et al., 2022a; Turgeon-Pelchat et al., 2021). These architectures include PointNet++ (Qi et al., 2017b), ConvPoint (Boulch, 2020), and PointCNN (Li et al., 2018). The Dynamic Graph CNN, or DGCNN (Wang et al., 2019), was selected for this study as it has been demonstrated to be a versatile and effective architecture across a variety of modelling tasks (Bello et al., 2020; Diab et al., 2022; Liu et al., 2022b). Like most point-based DNNs, DGCNN requires each input point cloud to have the same number of points (Liu et al., 2022b; Wang et al., 2019). This requirement was addressed by randomly downsampling input point clouds to the target number of points prior to each epoch. This random downsampling approach meant that each epoch, the model would view a slightly different set of points for each training point cloud, thus providing additional data augmentation. In contrast, validation and test datasets were downsampled using the farthest point sampling (FPS) approach to maintain their fidelity. FPS involves randomly selecting an initial starting point, repeatedly calculating the distance to all other points, and retaining the farthest point in each iteration until the target number of points is reached (Liu et al., 2022a). Although we did not perform a thorough investigation of the optimal number of points to use with DGCNN, early experimentation suggested that 5120 points per plot (13 pt/m^2) provided the best results. In plots that had fewer than 5120 returns, points were randomly sampled with replacement and duplicated with a small amount of noise until the target number was reached. Though DGCNN can operate using additional features such as surface normal vectors, DGCNN was applied in this study using only the XYZ coordinates as input features.

Fig. 2C summarizes key characteristics of DGCNN, including the type of input data and the learning mechanism. DGCNN is based on PointNet (Qi et al., 2017a), and learns from a point cloud by building a graph around a given point using the 20 nearest neighbor points. The graph used in DGCNN represents each neighboring point as a node and pairwise connections between points as edges. DGCNN then applies a specialized convolution-like operation called EdgeConv to the neighborhood graph to learn features. As the point cloud passes through DGCNN, the neighborhood graphs are dynamically updated for each point, allowing the model to learn the local and global point cloud structure. Finally, DGCNN uses a series of MLPs and pooling operations to summarize and extract information from the learned features to make predictions (Wang et al., 2019).

2.9. Hyperparameter configurations and model training

An important aspect of DL models is their sensitivity to hyperparameter configuration (Agrawal, 2021). Hyperparameters are the parameters that govern how a DNN learns, including but not limited to: learning rate, batch size, number of epochs, weight decay, and dropout probability. While many DL studies perform hyperparameter tuning for each model (e.g., Dimitrovski et al., 2023), this was not done in this study. This is because point cloud DNNs are demanding in terms of computational resources and require significant time and computer memory to train. For example, training times with the available computer resources in this study (two NVIDIA RTX A4000 GPUs, 16 GB memory each) required up to 37 h for 200 epochs. Instead of performing hyperparameter tuning, a single hyperparameter configuration was implemented for both DL models similar to that used by Oehmcke et al. (2022) which is shown in Table 2.

As shown in Equation (6), for additive AGB models, a customized Mean Squared Error (MSE) loss function was implemented to ensure that models evenly estimated biomass components while also encouraging additivity. MSE loss using only total AGB was implemented for direct AGB models. DNN parameter states were saved after each epoch if the validation loss was lower than any prior epoch. The DNN state that achieved the lowest loss (Eq. (2)) on the validation set was applied to the testing dataset to derive performance metrics. DNN training was implemented using the PyTorch package (v. 1.13.0) in Python (Paszke et al., 2019).

$$Loss = MSE_{Wood} + MSE_{Branch} + MSE_{Bark} + MSE_{Foliage} + MSE_{Tree}$$

Equation 6

Table 2
Hyperparameter configuration used to train the Dynamic Graph CNN and the Octree CNN-HRNet. This configuration was not derived from hyperparameter tuning, but was instead based on that used by Oehmcke et al. (2022). We used the AdamW optimizer and cosine annealing warm restarts learning rate scheduler developed by Loshchilov and Hutter (2019, 2017).

Hyperparameter	Value
Number of Training Data Augmentations	3
Initial Learning Rate	0.001
Batch Size	8
Number of Epochs	200
Dropout Probability	0.8
Optimizer	AdamW
Weight Decay	0.01
Learning Rate Scheduler	Cosine Annealing Warm Restarts
N iterations for first restart (T_0)	20
Increases after restart (T_{mult})	2

Unlike the DNNs implemented in this study, RF models are relatively fast to train, allowing for automated hyperparameter tuning regimes. The Optuna Python package (v. 3.2.0; Akiba et al., 2019) was used to perform a random hyperparameter search for RF over a 12 h time frame. Table 3 summarizes the hyperparameters included in the random search with their respective value ranges. The optimal hyperparameter configuration for RF was selected based on lowest tree RMSE on the validation dataset achieved by the additive biomass model.

2.10. Comparing models

Fig. 3 provides an overview of the methods implemented in this study to address the research questions. Two versions of each model were trained: one as a multi-output regressor estimating tree biomass components and subsequently additive AGB ($AGB_{Additive}$), and another as a single variable regressor estimating total AGB directly (AGB_{Direct}). Both the additive and direct AGB versions of each model were trained with the same hyperparameter configuration. Performance metrics were computed for all models using the testing dataset. For each target variable (wood, branch, bark, and foliage biomass, in addition to $AGB_{Additive}$ and AGB_{Direct}) three performance metrics were computed for comparison: the coefficient of determination (R^2), root mean square error (RMSE), and mean absolute percentage error (MAPE). These performance metrics were selected based on previous studies comparing DNNs to conventional ML for tree AGB estimation (Ayrey et al., 2021; Ayrey and Hayes, 2018; Oehmcke et al., 2022). To account for stochastic variation in model training inherent in DL and RF, each model was trained and tested three times for additive and direct AGB estimation using randomly initialized weights for the DNNs. For each performance metric, the mean and standard deviation were computed from the three training runs (reported in results as mean ± standard deviation). This provided confidence that the metrics captured a component of the variation in model performance given different random starting weights in the DNNs. Finally, the performance of the best model overall was evaluated by dominant species to identify model biases for different species. The dominant species in a given plot was determined based on species total AGB in that plot. Plots in the test dataset were grouped by dominant species and performance metrics were calculated separately for each species. Python code used for DNN architectures and model training is indexed with Zenodo (Seely, 2023) and is available the following link: https://github.com/harryseely/Biomass-DL.

3. Results

3.1. Random forest hyperparameter tuning

RF hyperparameter tuning implemented in Optuna evaluated a total of 4000 trial configurations over 12 h. RF performance did not vary substantially between trials, with an average RMSE of 30.2 Mg/ha and standard deviation of 1.2 Mg/ha. Hyperparameter tuning results showed that data augmentation did not benefit RF performance, with 0 augmentations to the training dataset yielding the best results. The optimal variable importance threshold was 0.005, which included 29–33 metrics for additive models, and 19–22 metrics for direct models (depending on the run). The most important features for direct and additive AGB models included mean height (zmean), 45th height percentile (zq45), height of median energy (HOME), voxel elevation standard deviation (vzsd), and the percentage of returns above 5 m (pzabove5).

Table 3
Tuning ranges for Random Forest (RF) random hyperparameter search and the best values identified from the search for each hyperparameter. Note that for maximum number of features for splitting a node, $n_{features}$ is the number of lidar metrics selected to be used in the model based on the variable importance threshold.

Parameter	Value Search Range	Best Value
Number of training data augmentations	0–5	0
Variable importance threshold	0–0.1	0.005
Number of estimators (trees)	100–3000	200
Max depth	80–110	90
Minimum number of samples per split	8–16	12
Minimum number of samples per leaf	3–5	4
Maximum number of features for splitting a node	1–3, $\sqrt{n_{features}}$, $\log_2(n_{features})$	1
Proportion of samples for bootstrap	0.5–1.0	0.9

3.2. Deep learning training

Fig. 4 shows the learning curves for the best performing training runs of the DGCNN and OCNN-HRNet additive and direct AGB models. DNN training achieved the best performance on the validation dataset (i.e., the model converged) between epochs 55 and 181 depending on the run. The generalization gap (i.e., difference between training and validation loss curves) was larger for OCNN-HRNet (Fig. 4 A, C) than for DGCNN (Fig. 4 B, D). DGCNN consistently had larger training loss than validation loss. OCNN-HRNet and DGCNN training with two GPUs required an average of 36.9 h (~11 min/epoch) and 16.5 h (~5 min/epoch), respectively. This training lasted 17,000 times longer on average compared to RF training time (~6 s with 16 CPU cores).

3.3. Additive versus direct AGB estimation

Additive and direct AGB estimation performed similarly when averaged across training runs, with the most notable differences expressed in terms of MAPE (Fig. 5). The difference between additive and direct models in terms of R^2 averaged across all models was minor (0.77 ± 0.005 for additive; 0.78 ± 0.003 for direct). The same was true of RMSE (26.9 Mg/ha ±0.3 Mg/ha for additive; 26.6 Mg/ha ±0.2 Mg/ha for direct). In terms of MAPE, additive models demonstrated an average 22% reduction compared to direct models (59.5 % ± 7.9 % and 81.6 % ± 18.8 %, respectively). This finding was most pronounced for DGCNN, which had an additive MAPE of 56.8 % ± 7.8% compared to a direct MAPE of 118.9 % ± 44.1% (difference of 62%). DGCNN additive models also outperformed direct models in terms of R^2 and RMSE, though this difference was smaller compared to that found for MAPE (Fig. 5). RF additive models provided an average 11% reduction in MAPE (69.3 % ± 0.8 % for additive; 80.6 % ± 3.0 % for direct). OCNN-HRNet additive models were outperformed by the direct models across all metrics on average. The most notable improvement afforded by the OCNN-HRNet direct model over the additive model was a RMSE reduction of 1 Mg/ha (26.6 Mg/ha ±0.3 Mg/ha for additive; 25.6 Mg/ha ±0.3 Mg/ha for direct).

3.4. Comparing RF and DNN models

As shown in Figs. 5 and 6, all three models performed similarly for estimating tree biomass, with OCNN-HRNet slightly outperforming DGCNN and RF, especially for direct AGB. The spread of residuals was similar across all three models, with residual error increasing for larger AGB values (Fig. 7). Fig. 7 also shows the presence of some outlier plots in the test dataset with large errors. As shown in Table 4, there are three performance metrics for each of the six target variables, comprising a total of 18 metrics averaged across training runs to compare between models (Table 4). Across all metrics, OCNN-HRNet performed best on average for 12/18, DGCNN for 2/18, and RF for 3/18. Together, DNNs outperformed RF across 15/18 metrics.

In terms of MAPE, OCNN-HRNet reduced error by 20% on average across all target variables (Table 4) compared to RF (56.5% ± 14.6 % for OCNN-HRNet; 76.7% ± 1.4% for RF). DGCNN did not demonstrate the same performance, only reducing MAPE by 2% on average compare to RF (74.1% ± 15.0% for DGCNN). R^2 and RMSE experienced less

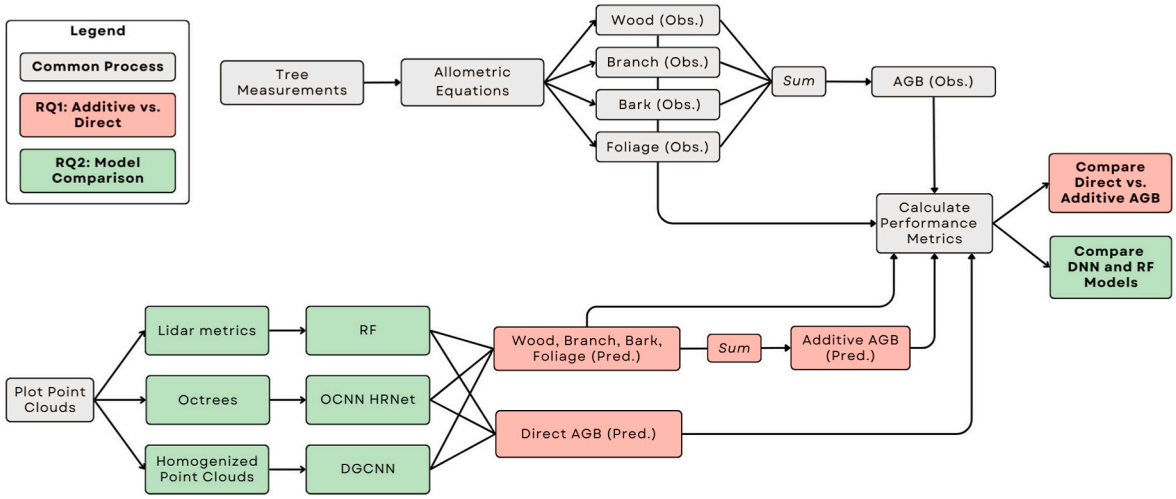

Fig. 3. Overview of approach for addressing the study objectives. Processes and outcomes focused on specific objectives are colour coded. Three models are compared for additive and direct aboveground biomass (AGB) estimation: Random Forest (RF), Octree CNN (OCNN) HRNet, and Dynamic Graph CNN (DGCNN). The "Obs." and "Pred." abbreviations represent observed and predicted biomass values. (For interpretation of the references to colour in this figure legend, the reader is referred to the Web version of this article.)

variation between the three models. The most notable differences in R^2 scores were for bark and foliage estimates. For bark estimates, OCNN-HRNet and DGCNN achieved R^2 scores of 0.79 (±0.006) and 0.77 (±0.008), compared the RF score of 0.48 (±0.009). For foliage estimates, RF outperformed both DNNs with an R^2 score of 0.75 (±0.003) compared to 0.66 (±0.015) and 0.53 (±0.061) for OCNN-HRNet and DGCNN, respectively. RMSE primarily differed for bark estimates, with OCNN-HRNet and DGCNN achieving 2.6 (±0.04) Mg/ha and 2.7 (±0.05) Mg/ha, respectively, compared to 4.3 (±0.04) Mg/ha for RF.

Overall, OCNN-HRNet was the best model in terms of additive and direct AGB estimation with an R^2 of 0.79 (±0.005) and 0.8 (±0.004), respectively. OCNN-HRNet biomass component estimation yielded R^2 ranging from 0.66 to 0.78 across wood, branch, bark, and foliage biomass estimates. Notably, OCNN-HRNet achieved an average Direct-AGB MAPE of 45.4% (±9.3%), providing a 35.1% improvement compared to that of RF (80.5% ± 3.0%).

3.5. Model performance by species

Model performance as represented by OCNN-HRNet (best overall model) varied by species and component (Fig. 8). Common species (dominant in 87% of plots) including fir, spruce, maple, birch, and aspen, had good model fits, with R^2 between 0.7 and 0.8. Less common species including cedar, pine, and beech (dominant in 10% of plots) had generally poorer and more variable model fits, with R^2 ranging between 0.4 and 0.8. Species that were rare in the dataset, including tamarack, alder, ash, hemlock, and poplar (dominant in only 4% of plots), yielded less accurate biomass predictions and had insufficient samples to provide reliable estimates of model fit. For all coniferous species, model fit for biomass components was good, with R^2 between 0.7 and 0.8. A similar trend was true for broadleaf species, except that model fit was poor for foliage, with R^2 of 0.07.

3.6. Applying DNN to map tree biomass

To demonstrate the inference capacity of OCNN-HRNet, we applied the model to a subset of the study area containing a variety of forest management regimes, species compositions, and biomass values (Fig. 9). It is apparent that tree component biomass is spatially correlated; however, in some areas the amount of biomass differs substantially between components. This pattern is highlighted in Fig. 10, which shows a Red–Green–Blue (RGB) colour composite generated using the normalized predicted branch, bark, and foliage biomass values. In Fig. 10 we can see that the Northwest of the subset area is dominated by branch and bark biomass, whereas the Southeast is dominated by foliage biomass.

4. Discussion

4.1. Modelling tree AGB using additive and direct approaches

This study compared additive and direct approaches to tree AGB estimation for RF and DNN models. Our results indicate that additive AGB models perform similarly to direct models, and in some cases even provide improved performance. Although additive models can result in a minor reduction in the accuracy of estimated total AGB in some cases, this approach provides significantly more information about tree biomass and carbon storage. As shown in Figs. 9 and 10, when mapped across the landscape, patterns in tree component biomass can reveal interesting structural characteristics of a forest which are less obvious when looking at a total AGB map. These findings are in line with a similar study by Sanquetta et al. (2015), which compared additive Seemingly Unrelated Regression (SUR) and direct regression of tree AGB. They found that both approaches yielded similar results, with the additive SUR demonstrating no significant reduction in AGB estimation accuracy compared to the direct approach.

By splitting tree biomass into individual components and calculating the MSE loss (Eq. (6)) for each of them separately, the DNN models are provided with additional information during training. These results suggest that they can make use of that information and understand that different parts of the point cloud correspond to different biomass components. Additionally, since the squared term in the loss function is applied to each component separately, large deviations in individual components are unlikely. This can be understood like a regularization term, where unrealistically large (or small) estimates for the components are discouraged. We also applied Z-score normalization to the biomass components to avoid biasing the models towards components with greater biomass (i.e., wood, branches). However, weighting the loss function (Eq. (6)) towards higher biomass contributors may be desirable in some cases, and is worth pursuing in future research.

4.2. Comparing random forest and deep learning models

This study evaluated whether point cloud DL can improve upon the

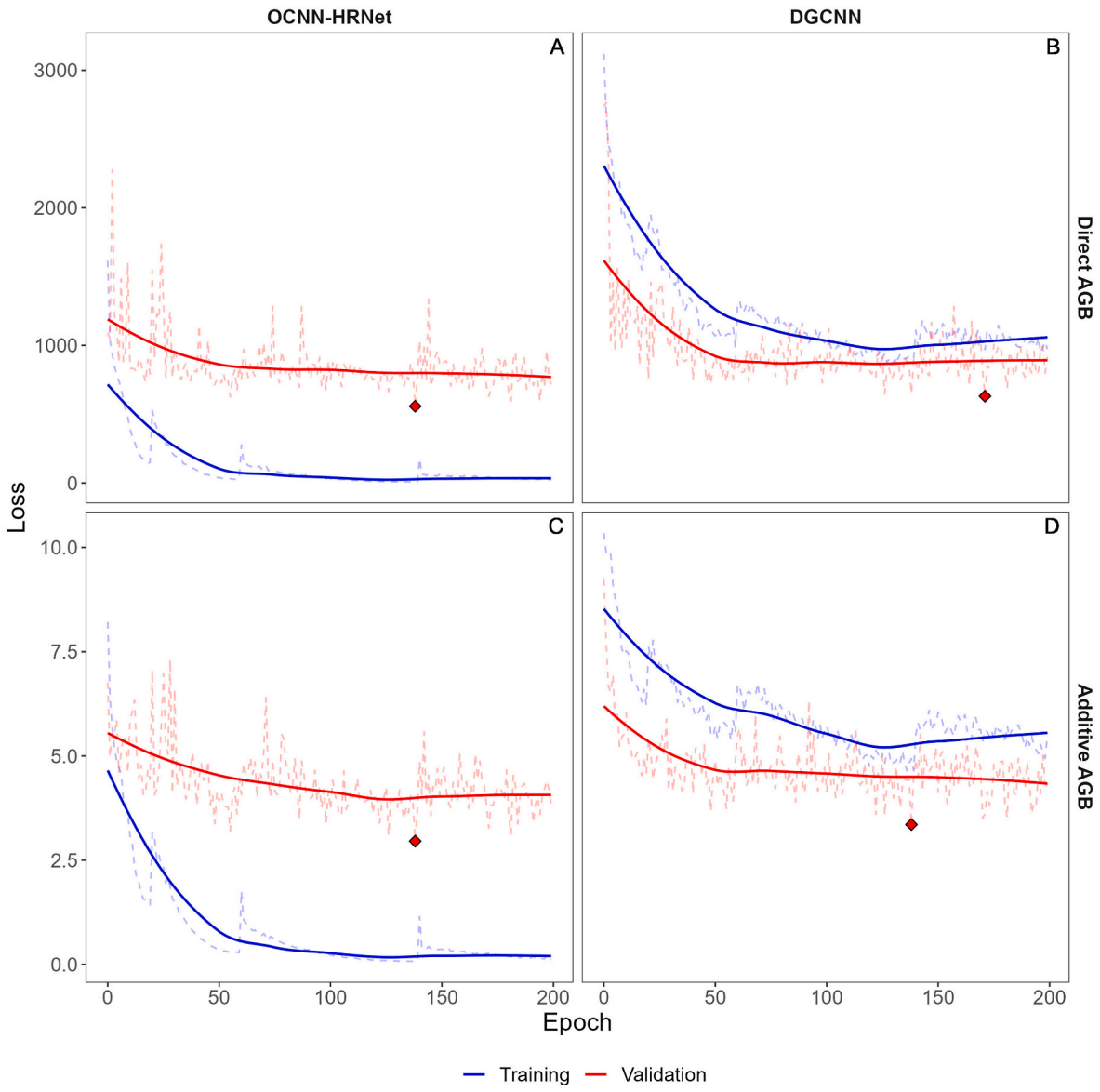

Fig. 4. Learning curves for the best training runs of Octree CNN (OCNN) HRNet (A, C) and Dynamic Graph CNN (DGCNN; B, D). Direct (A, B) and additive (C, D) aboveground (AGB) tree biomass models are shown. Note that the loss axis for additive AGB (C, D) represents a unitless value since the target is z-score normalized, whereas the direct AGB loss is mean squared error (MSE). The dashed line shows the observed loss and the bolded line shows the smoothed loss (moving average with a window size of 7). The red diamond represents the epoch where the model achieved the lowest loss on the validation dataset. (For interpretation of the references to colour in this figure legend, the reader is referred to the Web version of this article.)

use of conventional ML and lidar metrics by using the point cloud directly. The point-based DGCNN and octree based OCNN-HRNet were compared to RF which served as a baseline lidar metric model. Generally, the two DNNs implemented in this study outperformed RF for both additive and direct AGB estimation, with OCNN-HRNet providing the greatest improvement relative to RF. This improvement was most pronounced in terms of MAPE. However, it should be noted that MAPE experienced large standard deviations for both DNNs across the target variables due to random initial weights and the stochastic deep learning process. Though MAPE varied between DNN runs (Figs. 5 and 6), the standard deviation of MAPE for both DNNs was typically lower than the difference in MAPE relative to RF, indicating that this difference was significant. A similar study by Oehmcke et al. (2022) also observed a substantial improvement in MAPE for point cloud DNNs compared to conventional ML models using lidar metrics. The higher MAPE values observed for the RF model compared to the DNNs may be a result of the differences in model structure between RF and DNNs resulting in certain prediction biases (Hamraz et al., 2019). Overall, these results suggest that point cloud DNNs, especially OCNN based models, can outperform RF in terms of both additive and direct AGB estimation, and should be considered viable options for future lidar-based tree AGB modelling. These results also suggest that features learned from point cloud DNNs provide more effective predictors for tree AGB than conventional lidar metrics.

While the DNNs implemented in this study did outperform RF in general, they did not achieve the large performance gains that have been reported in prior research comparing DNN and RF forest attribute models (Ayrey et al., 2021; Ayrey and Hayes, 2018; Hamraz et al., 2019). For example, a 3D CNN implemented by Ayrey and Hayes (2018) for AGB estimation provided an R^2 of 0.69 compared to the RF R^2 of 0.61, whereas the differences in terms of R^2 between DNN and RF in this study were not as pronounced. This may be due to several reasons. One explanation is that error in the reference data (e.g., fieldwork errors, GPS mismatch) and the range of different lidar acquisitions (e.g.,

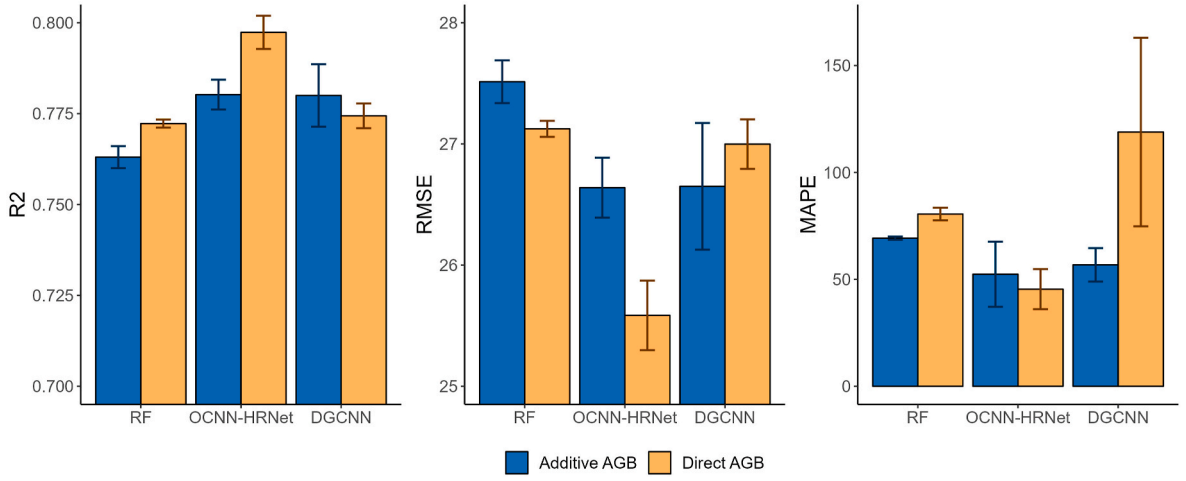

Fig. 5. Averaged performance metrics for additive versus direct approaches for modelling tree aboveground biomass (AGB) with Random Forest (RF), Octree CNN (OCNN) HRNet, and Dynamic Graph CNN (DGCNN). Error bars show the standard deviation of a given metric summarized across three training runs for each additive and direct AGB model.

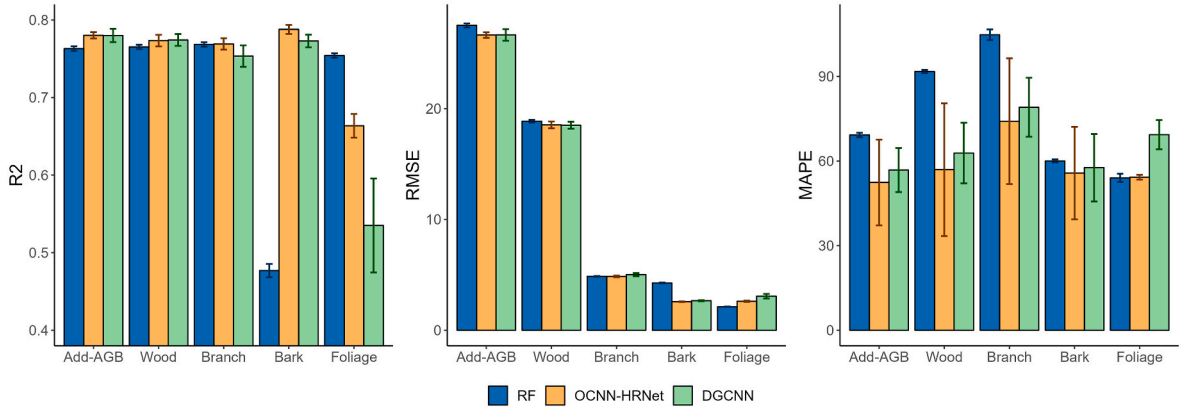

Fig. 6. Comparing performance metrics between Random Forest (RF), Octree CNN (OCNN)-HRNet, and Dynamic Graph CNN (DGCNN). Metrics are shown for tree biomass components and additive total aboveground biomass (Add-AGB). Error bars show the standard deviation of a given metric summarized across three training runs for each additive AGB model.

instrument and platform effects) may have negatively influenced the DNNs more than RF (Knott et al., 2023). RF is robust to noise and outliers due to its ensemble approach (Breiman, 2001) and lidar metrics may have added a smoothing effect by aggregating the points to statistical descriptors. In contrast, DNNs operating directly on the point cloud may be more sensitive to outliers, noise, and error in input reference data compared to RF. To that end, a recent study found that adding even a single outlier point to a point cloud can significantly reduce DNN performance (Tan and Kotthaus, 2023). Moreover, more complex data augmentation may also help reduce the effect of noise and outliers in point cloud data. For example, Li et al. (2020) implemented a generative adversarial network (GAN) which learns to optimize point cloud data augmentation on-the-fly during training. Future work should ensure that training data are appropriately pre-processed and adopt suitable data augmentation methods to minimize the negative effects of noise and outliers on point cloud DNN performance.

Another factor that may have narrowed the performance gap between DNNs and RF models in our study is the size of the training dataset. Ayrey and Hayes (2018) used a much larger training dataset consisting of 17,537 sample plots, which may have provided a more substantial benefit to their DNN compared to their RF model. The need for very large training datasets is a well studied concept in DL research, and may have been an important factor for the model comparison in this study (Hamedianfar et al., 2022; LeCun et al., 2015). Finally, the RF model implemented in this study was subject to rigorous hyperparameter tuning (4000 trials) to optimize performance, whereas DNN hyperparameters were pre-selected based on those used by Oehmcke et al. (2022) due to constraints imposed by lengthy DNN training times.

It is also useful to compare the point cloud DNNs implemented in this study to inform future application of such models. Across many point cloud DL tasks, point-based DNNs such as DGCNN typically outperform octree/voxel-based DNNs (Diab et al., 2022); however, this was not the case in this study. Notably, OCNN-HRNet outperformed DGCNN across 12 of the 18 metrics used in this study (Table 4). However, the improvements afforded by OCNN-HRNet compared to DGCNN were relatively small (Figs. 5 and 6). These minor improvements may be because OCNN-HRNet used additional features from the point cloud, such as intensity, return number, and scan angle, whereas DGCNN only used XYZ coordinates. Furthermore, OCNN-HRNet is a more complex model (3.6 M parameters) compared to DGCNN (2.1 M parameters). Ayrey and Hayes (2018) compared 3D CNNs with varying degrees of complexity and found that more complex models performed better for biomass regression. As such, additional complexity may have contributed to the performance gains of OCNN-HRNet.

The improved performance of the octree-based DNN compared to the point-based DNN is consistent with some prior studies dealing with ALS point clouds. For example, Oehmcke et al. (2022) found that a voxel-based DNN (Minkowski CNN) outperformed a point-based DNN

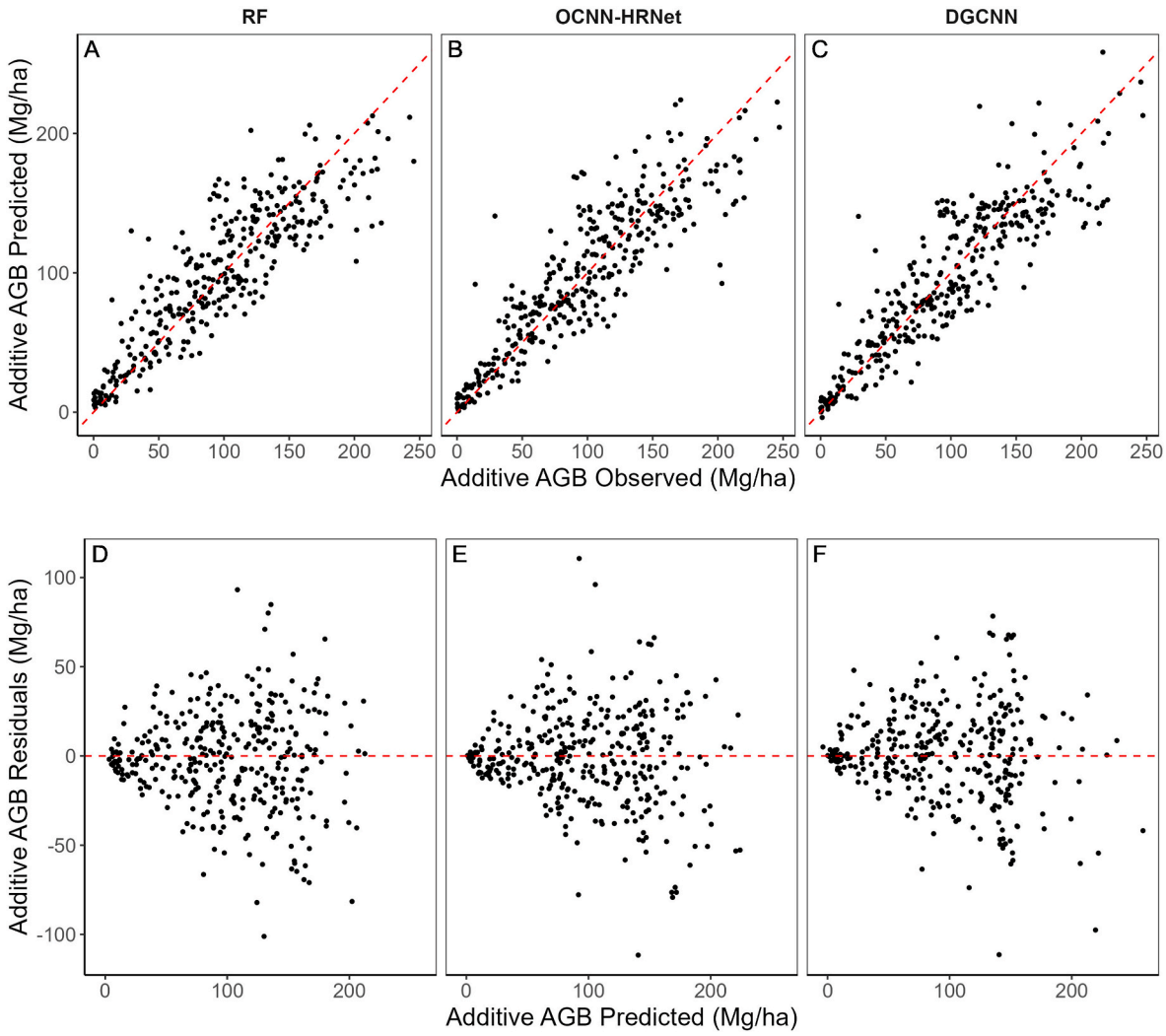

Fig. 7. Additive tree aboveground biomass (AGB) observed-predicted scatterplots (A, B, C) in addition to fitted-residual plots (D, E, F) for Random Forest (RF), Octree CNN (OCNN)-HRNet, and Dynamic Graph CNN (DGCNN). Predicted and residual values are taken from the best training run of each model.

(KPConv) for AGB estimation, with R^2 values of 0.81 and 0.79, respectively. Another study by Li et al. (2021) comparing DNNs for urban ALS point cloud classification found that the Submanifold Sparse CNN (voxel-based) outperformed PointNet++ and KPConv (both point-based) models by 1% and 5%, respectively. Overall, while point-based DNNs excel when applied to indoor point clouds (e.g., chairs, tables, lamps, etc.), there is increasing evidence that voxel or octree-based methods are better suited for forest point clouds, especially when acquired with ALS.

4.3. *Understanding biomass error by species*

A key benefit to modelling tree component biomass is the capacity to compare which biomass components contribute error for different species. This study highlighted several interesting error patterns for different dominant species in the plot data. For example, coniferous species had improved model fit for foliage compared to deciduous species (Fig. 8). This finding may be due to several factors, such as deciduous species typically having less accurate allometric equations for foliage (Lambert et al., 2005; Ung et al., 2008). In addition, residuals for all broadleaf dominated plots show that total AGB was underestimated by 5.4 Mg/ha on average, whereas coniferous dominated plots demonstrated overestimated total AGB by 1.2 Mg/ha on average. There are several possible explanations for these outcomes such as different canopy structures and leaf traits between tree species. It is also possible that lidar acquisition timing (Table 1) influenced the underestimation of broadleaf tree biomass since some acquisitions ranged from September to October during foliage senescence. Other interesting patterns in species biomass component error included plots dominated by maple exhibiting large residuals for branch, bark and foliage estimates compared to relatively low residuals for wood estimates. In contrast, plots dominated by fir exhibited the largest residuals for wood. Investigating biomass component error patterns by species can help modellers diagnose species specific biases in their model. Similarly, this knowledge can help identify potential issues with ground reference data or allometric equations (Vorster et al., 2020).

The substantial variation in model performance between different tree species highlights the importance of including species information in tree biomass models. For example, Latifi et al. (2015) demonstrated that stratifying their tree biomass model using species groups (conifer, deciduous, mixed) allowed their model to explain 11% more variation in biomass. Providing information about species to DNN and RF models may help account for species specific biases, and improve model performance overall.

4.4. *Study limitations*

An important limitation of the DNNs implemented in this study is the

Table 4
Regression metrics for Random Forest (RF), Octree CNN (OCNN)-HRNet, and Dynamic Graph CNN (DGCNN), averaged across three training runs. Metrics include the coefficient of determination (R^2), Root Mean Square Error (RMSE), and Mean Absolute Percentage Error (MAPE). The best performing metric across the three models is shaded in grey. Add-AGB represents the additive AGB model whereas Direct-AGB represents the direct model.

Metric	Component	RF	OCNN-HRNet	DGCNN
R^2	**Direct-AGB**	0.772	0.797	0.774
	Add-AGB	0.763	0.780	0.780
	Wood	0.765	0.773	0.774
	Branch	0.768	0.769	0.753
	Bark	0.477	0.788	0.773
	Foliage	0.754	0.664	0.535
RMSE	**Direct-AGB**	27.125	25.585	26.998
	Add-AGB	27.513	26.639	26.650
	Wood	18.869	18.540	18.506
	Branch	4.865	4.858	5.019
	Bark	4.267	2.577	2.666
	Foliage	2.124	2.619	3.075
MAPE	**Direct-AGB**	80.547	45.417	118.9
	Add-AGB	69.258	52.393	56.790
	Wood	91.723	56.926	62.825
	Branch	104.762	74.101	79.063
	Bark	60.027	55.706	57.618
	Foliage	54.007	54.218	69.354

lack of hyperparameter tuning. Hyperparameter tuning is an essential aspect of applying DNNs, but requires large amounts of time and computational resources (Hamedianfar et al., 2022). The trade-off between resources and performance is important to consider when comparing DNNs with conventional ML models such as RF which can be trained rapidly. Some experimentation with hyperparameters for OCNN-HRNet and DGCNN such as learning rate, batch size, and dropout rate, was observed to have a significant impact on model performance. However, this study ultimately adopted a hyperparameter configuration described in previous work by Oehmcke et al. (2022), and in-depth hyperparameter tuning for OCNN-HRNet and DGCNN may have resulted in improved outcomes. Due to long DNN training times (16–37 h using 2 GPUs), performing an effective hyperparameter search could require hundreds of hours of compute time, and was not feasible in this study. Future work in this area should explore more efficient methods for hyperparameter optimization, such as only using a subset of the training data for hyperparameter tuning or implementing early stopping (DeCastro-García et al., 2019). For a more reasonable model comparison, each model should undergo comparable hyperparameter tuning regimes.

Another limitation in this study was the risk of DNN overfitting. DNNs are more susceptible to overfitting compared to other models such as RF due to the large number of trainable parameters (Hamedianfar et al., 2022). Complex DNNs trained on a relatively small dataset can memorize the training data, thus resulting in an overfit model that does not generalize to the test dataset. Multiple regularization techniques were implemented in this study to limit overfitting, including the use of small batch sizes (8 samples), high dropout (80%), and learning rate scheduling (Table 2). Despite these efforts, as can be seen in Fig. 4, the generalization gap (difference between validation and training learning curves) was wide for OCNN-HRNet. In contrast, the DGCNN validation loss was actually lower (better) than the training loss. This unexpected outcome may be an artifact of the high dropout rate (80%) implemented in this study. The need for multiple regularization methods to limit overfitting suggests that the DNNs used in this study may be overly complex for the task of tree component biomass regression. Hamedianfar et al. (2022) argue that complex DNNs may be less suited for 1-dimensional modelling tasks such as regression, and are better suited for 2D or 3D tasks such as image or point cloud segmentation. It is possible that implementing a simpler DNN for tree biomass estimation may be more effective than the models evaluated in this study.

Another important limitation in this research is the rigid input data formats needed for point-based and octree-based DNNs. For DGCNN, input point clouds had to be downsampled to a specific number of points, and for OCNN-HRNet point clouds were converted to octrees with a minimum octant size of 34 cm on average. The conversion of the original point clouds to useable formats may have hindered the capacity of the DNNs to effectively model tree biomass. Although the number of

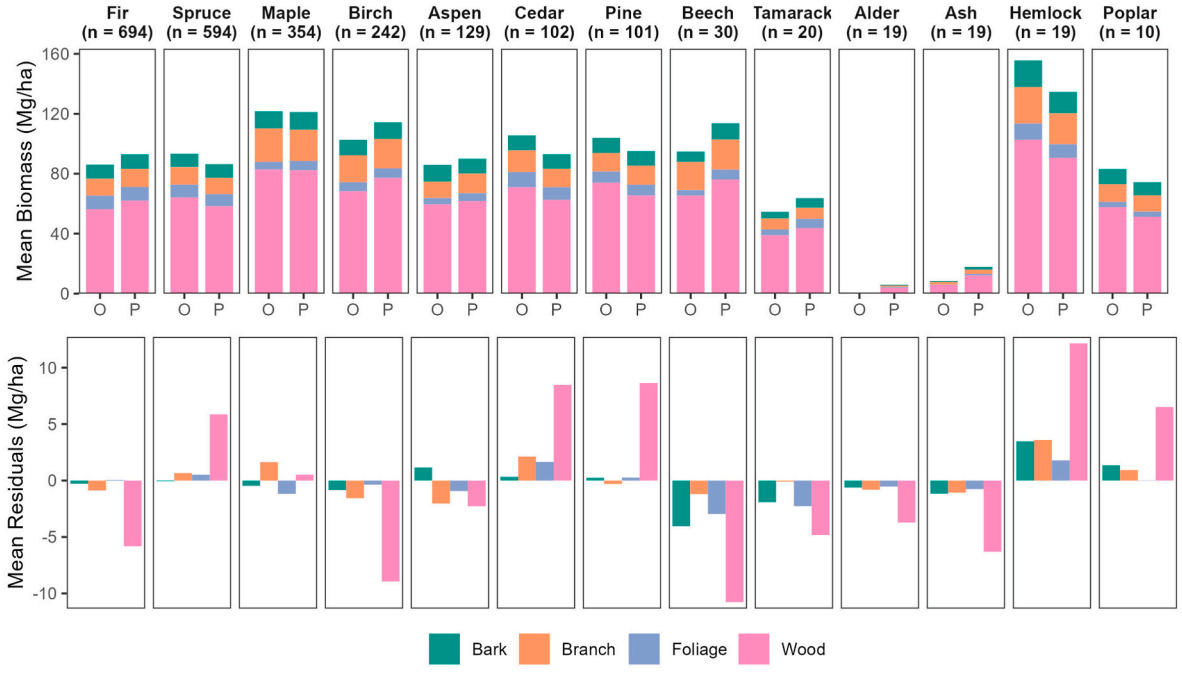

Fig. 8. Observed (O), predicted (P) and residual biomass component values in tons per hectare (Mg/ha) for OCNN-HRNet averaged by dominant species across all the test plots. Observed and predicted values from OCNN-HRNet are taken from the best training run of the model. The number of plots shown beneath each species name is the total number of plots across the training, validation, and testing datasets.

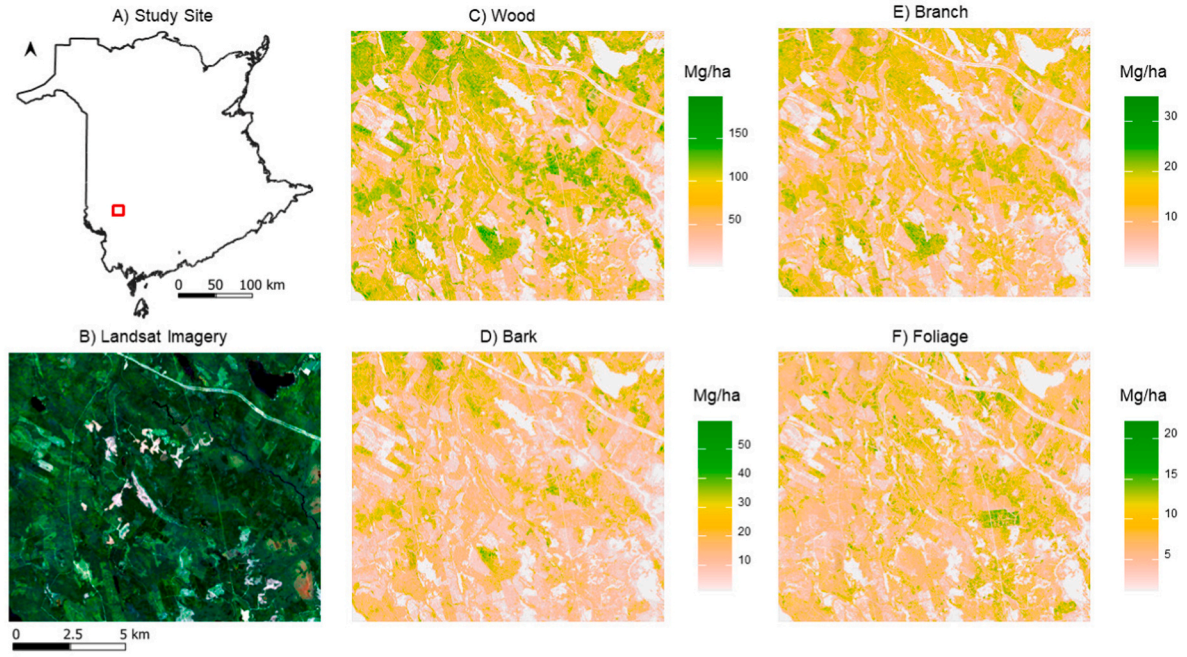

Fig. 9. Predicted tree component biomass maps generated using OCNN-HRNet for a subset of the study area shown in panel A in red. Panel B shows a Landsat-8 true colour composite from 2018 (same year lidar was collected in the area). Panels C – F show the predicted biomass for each component across the subset area at a 22.56 m resolution. Areas where the 95th height percentile is below 1.5 m are assumed to have no significant tree biomass and are shown in white. (For interpretation of the references to colour in this figure legend, the reader is referred to the Web version of this article.)

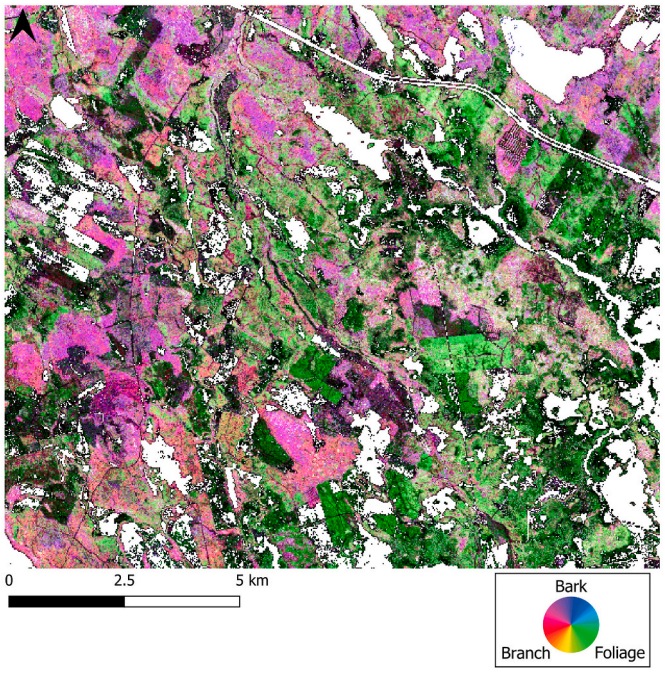

Fig. 10. Red–Green–Blue (RGB) colour composite generated for a subset of the study area using the predicted bark, branch, and foliage biomass values from OCNN-HRNet. The biomass of each component is normalized and then assigned to a colour channel (branch-red, foliage-green, and bark-blue). (For interpretation of the references to colour in this figure legend, the reader is referred to the Web version of this article.)

points in each plot varied from 5000 to 12,000, each point cloud was downsampled to 5120 points to be used in DGCNN as this provided the best results in early experiment. However, it should be noted that a different number of points may have provided better results given a different hyperparameter configuration. A study by Liu et al. (2022a) performing tree species classification on backpack laser scanning data compared the effect on the number of points on PointNet++ performance. The authors found that when PointNet++ was trained using between 1024 and 9216 points per sample, the model performed best with 3072 points. A similar experiment could be used to identify the optimal number of points for DGCNN when applied to biomass regression. Likewise, identifying the optimal octree depth (i.e., changing the size of the smallest possible octant) could improve the performance of OCNN-HRNet. While it was beyond the scope of this study to investigate the optimal number of points for DGCNN or octree depth for OCNN-HRNet, optimizing the input data structure likely has the potential to improved point cloud DNN performance.

4.5. *Future research*

The current body of research applying point cloud DL for tree biomass regression is limited (Ayrey et al., 2021; Ayrey and Hayes, 2018; Oehmcke et al., 2022). This is likely because DNNs are not commonly designed for or applied to regression tasks (Letzgus et al., 2022). In contrast, there is an increasingly large body of research that applies point cloud DNNs to many forest modelling tasks involving classification and segmentation (e.g., Hamraz et al., 2019; Krisanski et al., 2021a, 2021b; Liu et al., 2022a). As such, there is potential for repurposing models developed for forest classification and segmentation tasks to new regression tasks such as tree biomass estimation. Beyond adapting DNNs found in other research, there are several other areas that should be explored in future research.

Unlike this study, which used a single data source (ALS), many contemporary studies modelling tree biomass using remote sensing adopt a data fusion approach (e.g., Luo et al., 2017; Zhang et al., 2019). Data fusion has been shown to improve modelling accuracy by overcoming single data source shortcomings (Fassnacht et al., 2014). Data fusion models combine multiple sources of active and passive remote sensing data such as radar, lidar, multispectral, and hyperspectral, in addition to ancillary datasets, such as stand age, species composition,

disturbance history, and climate information in a unified model (Ghamisi et al., 2019). For example, Zeng et al. (2022) used lidar metrics in combination with X-band SAR data in an OLS model to estimate tree biomass components in China. The authors observed that combining both data sources improved the lidar-only model R^2 from 0.46 to 0.82.

Adopting a data fusion approach could improve the capacity of point DNNs to estimate tree biomass by contextualizing features learned by a point cloud DNN. Features learned from the point cloud could be further refined based on the climatic history of the area, spectral reflectance, and other characteristics relating to tree biomass. However, one key barrier to data fusion in point cloud deep learning is the way in which additional datasets are incorporated into a DNN. Several studies have proposed novel ways of doing this. For example, Chang et al. (2019) developed a DNN that uses Landsat and aerial imagery in combination with terrain and climate data in multiple branches of CNNs and DenseNets (Huang et al., 2017) to perform forest attribute regression. An alternative approach by Zhang et al. (2019) implemented a stacked sparse autoencoder DNN which fused Landsat derived spectral indices and lidar derived metrics to estimate forest AGB. The approaches developed in these studies could be adapted to include point cloud DNNs such as DGCNN or OCNN-HRNet instead of CNNs or autoencoders.

A final area of research that is critical for the improvement of point cloud DNNs for forest biomass regression is DL explainability. Explainability in the context of DL refers to our ability to understand how and why a model makes a certain prediction (Nguyen et al., 2022). For point cloud DNNs, an example of explainability could be identifying patterns in the point cloud, such as neighborhoods of points, that are most important for predicting a certain biomass value. In the case of foliage biomass estimation, one could visualize point importance to determine if the model is placing more importance on points located in the tree canopy. If all the important points for foliage estimation are ground returns, this may indicate that a model is not learning effectively. Without the capacity to explain a DNN, it becomes difficult to trace sources of error in the model and to determine whether the model is learning properly (i.e., making logical decisions). This “black box” nature ultimately limits the usefulness of DNNs in real world applications.

There has been progress in recent years towards explainable DL, with the development of frameworks such as LIME (Ribeiro et al., 2016) and DeepLIFT (Shrikumar et al., 2017) that can highlight important features in a trained DNN. Some methods have even been adapted specifically for point cloud DNNs (e.g., Tan and Kotthaus, 2022; Zhou et al., 2016). For example, Liu et al. (2022b) used class activation mapping (CAM; Zhou et al., 2016) in a study classifying tree species with point cloud DNNs to visualize which points were most important to the model’s decision. Despite the growing uptake of explainable DL methods for classification tasks, there remains a lack of similar methods for regression tasks (Letzgus et al., 2022). This is because it is easier to relate specific DNN features to categorical outputs than it is to do so for quantitative numeric outputs. Overall, the usefulness of point cloud DNNs for regression will remain limited until advances are made in explainable DL regression.

5. Conclusions

This study compared direct and additive approaches for tree AGB estimation using RF and DNN models. Additive AGB estimation performed similarly and, in some cases, better than direct AGB estimation. This finding supports the use of additive AGB models in future research and practice. The point cloud DNNs implemented in this study outperformed RF for additive and direct biomass estimation. However, the performance gains were not as substantial as those observed in previous studies. We suspect that larger training datasets, hyperparameter tuning, and data fusion will lead to better performance from point cloud DNNs going forward. Moreover, improved methods for explaining point cloud DNNs will improve our capacity to identify flaws with deep learning methods and to trace model error.

Funding

This research was undertaking in collaboration with Natural Resources Canada. This work is supported by the National Research Council of Canada (NRC; under project number DHGA-119-1); and partly by the Natural Sciences and Engineering Research Council of Canada (NSERC; under grant RGPIN-2018-03851).

Author contribution statement

Conceptualization: H.S., N.C.C., J.C.W, and A.R.; Data curation: H.S.; Formal Analysis: H.S.; Funding acquisition: N.C.C., J.C.W, and A.R.; Investigation: H.S. and N.C.C.; Methodology: H.S., N.C.C., J.C.W, D.M., L.W., and A.R.; Software: H.S. and L.W.; Supervision: N.C.C. Visualization: H.S.; Writing – original draft: H.S., N.C.C., J.C.W, D.M., L.W., and A.R.; Writing – review & editing: H.S., N.C.C., J.C.W, D.M., L.W., and A.R..

Declaration of competing interest

The authors declare that they have no known competing financial interests or personal relationships that could have appeared to influence the work reported in this paper.

Data availability

Lidar is available at GeoNB website. CLI plot data is available upon request from the Gov. of NB. Code at https://github.com/harryseely/Biomass-DL.

Acknowledgements:

We thank Chris Hennigar and Adam Dick for assistance with preprocessing the New Brunswick plot and lidar data and Brent Murray for technical assistance in model development.

Appendix A. Supplementary data

Supplementary data to this article can be found online at https://doi.org/10.1016/j.srs.2023.100110.

References

Affleck, D.L.R., Diéguez-Aranda, U., 2016. Additive nonlinear biomass equations: a likelihood-based approach. For. Sci. 62, 129–140. https://doi.org/10.5849/forsci.15-126.

Agrawal, T., 2021. Introduction to hyperparameters. In: Agrawal, T. (Ed.), Hyperparameter Optimization in Machine Learning: Make Your Machine Learning and Deep Learning Models More Efficient. Apress, Berkeley, CA, pp. 1–30. https://doi.org/10.1007/978-1-4842-6579-6_1.

Akiba, T., Sano, S., Yanase, T., Ohta, T., Koyama, M., 2019. Optuna: a next-generation hyperparameter optimization framework. In: Proceedings of the 25th ACM SIGKDD International Conference on Knowledge Discovery & Data Mining, KDD ’19. Association for Computing Machinery, New York, NY, USA, pp. 2623–2631. https://doi.org/10.1145/3292500.3330701.

Alzubaidi, L., Zhang, J., Humaidi, A.J., Al-Dujaili, A., Duan, Y., Al-Shamma, O., Santamaría, J., Fadhel, M.A., Al-Amidie, M., Farhan, L., 2021. Review of deep learning: concepts, CNN architectures, challenges, applications, future directions. Journal of Big Data 8, 53. https://doi.org/10.1186/s40537-021-00444-8.

Ayrey, E., Hayes, D.J., 2018. The use of three-dimensional convolutional neural networks to interpret LiDAR for forest inventory. Rem. Sens. 10, 649. https://doi.org/10.3390/rs10040649.

Ayrey, E., Hayes, D.J., Kilbride, J.B., Fraver, S., Kershaw, J.A., Cook, B.D., Weiskittel, A. R., 2021. Synthesizing disparate LiDAR and satellite datasets through deep learning to generate wall-to-wall regional inventories for the complex, mixed-species forests of the eastern United States. Rem. Sens. 13 https://doi.org/10.3390/rs13245113.

Belgiu, M., Drăguţ, L., 2016. Random forest in remote sensing: a review of applications and future directions. ISPRS J. Photogrammetry Remote Sens. 114, 24–31. https://doi.org/10.1016/j.isprsjprs.2016.01.011.

Bello, S.A., Yu, S., Wang, C., Adam, J.M., Li, J., 2020. Review: deep learning on 3D point clouds. Rem. Sens. 12, 1729. https://doi.org/10.3390/rs12111729.

Benomar, L., DesRochers, A., Larocque, G.R., 2012. The effects of spacing on growth, morphology and biomass production and allocation in two hybrid poplar clones

growing in the boreal region of Canada. Trees (Berl.) 26, 939–949. https://doi.org/10.1007/s00468-011-0671-6.
Bloom, A.A., Exbrayat, J.-F., van der Velde, I.R., Feng, L., Williams, M., 2016. The decadal state of the terrestrial carbon cycle: global retrievals of terrestrial carbon allocation, pools, and residence times. Proc. Natl. Acad. Sci. USA 113, 1285–1290. https://doi.org/10.1073/pnas.1515160113.
Boulch, A., 2020. ConvPoint: Continuous convolutions for point cloud processing. Comput. Graph. 88, 24–34. https://doi.org/10.1016/j.cag.2020.02.005.
Breiman, L., 2001. Random forests. Mach. Learn. 45, 5–32. https://doi.org/10.1023/A:1010933404324.
Briechle, S., Krzystek, P., Vosselman, G., 2021. Silvi-Net – a dual-CNN approach for combined classification of tree species and standing dead trees from remote sensing data. Int. J. Appl. Earth Obs. Geoinf. 98, 102292 https://doi.org/10.1016/j.jag.2020.102292.
Chang, T., Rasmussen, B.P., Dickson, B.G., Zachmann, L.J., 2019. Chimera: a multi-task recurrent convolutional neural network for forest classification and structural estimation. Rem. Sens. 11, 768. https://doi.org/10.3390/rs11070768.
Choy, C., Gwak, J., Savarese, S., 2019. 4D Spatio-Temporal ConvNets: Minkowski Convolutional Neural Networks. https://doi.org/10.48550/arXiv.1904.08755.
Cosenza, D.N., Korhonen, L., Maltamo, M., Packalen, P., Strunk, J.L., Næsset, E., Gobakken, T., Soares, P., Tomé, M., 2021. Comparison of linear regression, k-nearest neighbour and random forest methods in airborne laser-scanning-based prediction of growing stock. Forestry: Int. J. Financ. Res. 94, 311–323. https://doi.org/10.1093/forestry/cpaa034.
DeCastro-García, N., Muñoz Castañeda, Á.L., Escudero García, D., Carriegos, M.V., 2019. Effect of the sampling of a dataset in the hyperparameter optimization phase over the efficiency of a machine learning algorithm. Complexity 2019.
Diab, A., Kashef, R., Shaker, A., 2022. Deep learning for LiDAR point cloud classification in remote sensing. Sensors 22, 7868. https://doi.org/10.3390/s22207868.
Dimitrovski, I., Kitanovski, I., Kocev, D., Simidjievski, N., 2023. Current Trends in Deep Learning for Earth Observation: an Open-Source Benchmark Arena for Image Classification. https://doi.org/10.48550/arXiv.2207.07189.
Domingo, D., Montealegre, A.L., Lamelas, M.T., García-Martín, A., de la Riva, J., Rodríguez, F., Alonso, R., 2019. Quantifying forest residual biomass in Pinus halepensis Miller stands using Airborne Laser Scanning data. GIScience Remote Sens. 56, 1210–1232. https://doi.org/10.1080/15481603.2019.1641653.
Dong, L., Zhang, L., Li, F., 2016. Allometry and partitioning of individual tree biomass and carbon of Abies nephrolepis Maxim in northeast China. Scand. J. For. Res. 31, 399–411. https://doi.org/10.1080/02827581.2015.1060257.
Duncanson, L., Armston, J., Disney, M., Avitabile, V., Barbier, N., Calders, K., Carter, S., Chave, J., Herold, M., Crowther, T.W., Falkowski, M., Kellner, J.R., Labrière, N., Lucas, R., MacBean, N., McRoberts, R.E., Meyer, V., Næsset, E., Nickeson, J.E., Paul, K.I., Phillips, O.L., Réjou-Méchain, M., Román, M., Roxburgh, S., Saatchi, S., Schepaschenko, D., Scipal, K., Siqueira, P.R., Whitehurst, A., Williams, M., 2019. The importance of consistent global forest aboveground biomass product validation. Surv. Geophys. 40, 979–999. https://doi.org/10.1007/s10712-019-09538-8.
Duncanson, L., Neuenschwander, A., Hancock, S., Thomas, N., Fatoyinbo, T., Simard, M., Silva, C.A., Armston, J., Luthcke, S.B., Hofton, M., Kellner, J.R., Dubayah, R., 2020. Biomass estimation from simulated GEDI, ICESat-2 and NISAR across environmental gradients in Sonoma County, California. Rem. Sens. Environ. 242, 111779 https://doi.org/10.1016/j.rse.2020.111779.
Fassnacht, F.E., Hartig, F., Latifi, H., Berger, C., Hernández, J., Corvalán, P., Koch, B., 2014. Importance of sample size, data type and prediction method for remote sensing-based estimations of aboveground forest biomass. Rem. Sens. Environ. 154, 102–114. https://doi.org/10.1016/j.rse.2014.07.028.
García, M., Riaño, D., Chuvieco, E., Danson, F.M., 2010. Estimating biomass carbon stocks for a Mediterranean forest in central Spain using LiDAR height and intensity data. Rem. Sens. Environ. 114, 816–830. https://doi.org/10.1016/j.rse.2009.11.021.
GeoNB, 2022. GeoNB Data Catalogue [WWW Document]. URL. http://www.snb.ca/geonb1/e/DC/catalogue-E.asp. accessed 7.8.22.
Ghamisi, P., Rasti, B., Yokoya, N., Wang, Q., Hofle, B., Bruzzone, L., Bovolo, F., Chi, M., Anders, K., Gloaguen, R., Atkinson, P.M., Benediktsson, J.A., 2019. Multisource and multitemporal data fusion in remote sensing: a comprehensive review of the state of the art. IEEE Geoscience and Remote Sensing Magazine 7, 6–39. https://doi.org/10.1109/MGRS.2018.2890023.
Hamedianfar, A., Mohamedou, C., Kangas, A., Vauhkonen, J., 2022. Deep learning for forest inventory and planning: a critical review on the remote sensing approaches so far and prospects for further applications. Forestry: Int. J. Financ. Res. 95, 451–465. https://doi.org/10.1093/forestry/cpac002.
Hamraz, H., Jacobs, N.B., Contreras, M.A., Clark, C.H., 2019. Deep learning for conifer/deciduous classification of airborne LiDAR 3D point clouds representing individual trees. ISPRS J. Photogrammetry Remote Sens. 158, 219–230. https://doi.org/10.1016/j.isprsjprs.2019.10.011.
Hell, M., Brandmeier, M., Briechle, S., Krzystek, P., 2022. Classification of tree species and standing dead trees with lidar point clouds using two deep neural networks: PointCNN and 3DmFV-net. Photogramm. Fernerkund. GeoInf. 90, 103–121. https://doi.org/10.1007/s41064-022-00200-4.
Huang, G., Liu, Z., van der Maaten, L., Weinberger, K.Q., 2017. Densely Connected Convolutional Networks. Presented at the Proceedings of the IEEE Conference on Computer Vision and Pattern Recognition, pp. 4700–4708.
Jang, H.-J., Cho, K.-O., 2019. Applications of deep learning for the analysis of medical data. Arch Pharm. Res. (Seoul) 42, 492–504. https://doi.org/10.1007/s12272-019-01162-9.
Kankare, V., Vauhkonen, J., Holopainen, M., Vastaranta, M., Hyyppä, J., Hyyppä, H., Alho, P., 2015. Sparse density, leaf-off airborne laser scanning data in aboveground biomass component prediction. Forests 6, 1839–1857. https://doi.org/10.3390/f6061839.
Kanmegne Tamga, D., Latifi, H., Ullmann, T., Baumhauer, R., Bayala, J., Thiel, M., 2023. Estimation of aboveground biomass in agroforestry systems over three climatic regions in West Africa using Sentinel-1, Sentinel-2, ALOS, and GEDI Data. Sensors 23, 349. https://doi.org/10.3390/s23010349.
Knott, J.A., Liknes, G.C., Giebink, C.L., Oh, S., Domke, G.M., McRoberts, R.E., Quirino, V.F., Walters, B.F., 2023. Effects of outliers on remote sensing-assisted forest biomass estimation: a case study from the United States national forest inventory. Methods Ecol. Evol. https://doi.org/10.1111/2041-210X.14084 n/a.
Kotivuori, E., Korhonen, L., Packalen, P., 2016. Nationwide airborne laser scanning based models for volume, biomass and dominant height in Finland. Silva Fenn. 50.
Krisanski, S., Taskhiri, M.S., Gonzalez Aracil, S., Herries, D., Muneri, A., Gurung, M.B., Montgomery, J., Turner, P., 2021a. Forest structural complexity tool—an open source, fully-automated tool for measuring forest point clouds. Rem. Sens. 13, 4677. https://doi.org/10.3390/rs13224677.
Krisanski, S., Taskhiri, M.S., Gonzalez Aracil, S., Herries, D., Turner, P., 2021b. Sensor agnostic semantic segmentation of structurally diverse and complex forest point clouds using deep learning. Rem. Sens. 13, 1413. https://doi.org/10.3390/rs13081413.
Kristensen, T., Næsset, E., Ohlson, M., Bolstad, P.V., Kolka, R., 2015. Mapping above- and below-ground carbon pools in boreal forests: the case for airborne lidar. PLoS One 10, e0138450. https://doi.org/10.1371/journal.pone.0138450.
Krizhevsky, A., Sutskever, I., Hinton, G.E., 2012. Imagenet classification with deep convolutional neural networks. Adv. Neural Inf. Process. Syst. 25.
Kumar, A., Adamopoulos, S., Jones, D., Amiandamhen, S.O., 2021. Forest biomass availability and utilization potential in Sweden: a review. Waste Biomass Valor 12, 65–80. https://doi.org/10.1007/s12649-020-00947-0.
Kursa, M.B., Rudnicki, W.R., 2010. Feature selection with the Boruta package. J. Stat. Software 36, 1–13.
Kurz, W.A., Dymond, C.C., White, T.M., Stinson, G., Shaw, C.H., Rampley, G.J., Smyth, C., Simpson, B.N., Neilson, E.T., Trofymow, J.A., Metsaranta, J., Apps, M.J., 2009. CBM-CFS3: a model of carbon-dynamics in forestry and land-use change implementing IPCC standards. Ecol. Model. 220, 480–504. https://doi.org/10.1016/j.ecolmodel.2008.10.018.
Lambert, M., Ung, C.-H., Raulier, F., 2005. Canadian national tree aboveground biomass equations. Can. J. For. Res. 35, 1996–2018.
Latifi, H., Fassnacht, F.E., Hartig, F., Berger, C., Hernández, J., Corvalán, P., Koch, B., 2015. Stratified aboveground forest biomass estimation by remote sensing data. Int. J. Appl. Earth Obs. Geoinf. 38, 229–241. https://doi.org/10.1016/j.jag.2015.01.016.
LeCun, Y., Bengio, Y., Hinton, G., 2015. Deep learning. Nature 521, 436–444. https://doi.org/10.1038/nature14539.
Letzgus, S., Wagner, P., Lederer, J., Samek, W., Müller, K.-R., Montavon, G., 2022. Toward explainable AI for regression models. IEEE Signal Process. Mag. 39, 40–58. https://doi.org/10.1109/MSP.2022.3153277.
Li, N., Kähler, O., Pfeifer, N., 2021. A comparison of deep learning methods for airborne lidar point clouds classification. IEEE J. Sel. Top. Appl. Earth Obs. Rem. Sens. 14, 6467–6486. https://doi.org/10.1109/JSTARS.2021.3091389.
Li, R., Li, X., Heng, P.-A., Fu, C.-W., 2020. PointAugment: an auto-augmentation framework for point cloud classification. In: 2020 IEEE/CVF Conference on Computer Vision and Pattern Recognition (CVPR). Presented at the 2020 IEEE/CVF Conference on Computer Vision and Pattern Recognition (CVPR), pp. 6377–6386. https://doi.org/10.1109/CVPR42600.2020.00641.
Li, Y., Bu, R., Sun, M., Wu, W., Di, X., Chen, B., 2018. PointCNN: convolution on X-transformed points. In: Advances in Neural Information Processing Systems. Curran Associates, Inc.
Liu, B., Chen, S., Huang, H., Tian, X., 2022a. Tree species classification of backpack laser scanning data using the PointNet++ point cloud deep learning method. Rem. Sens. 14, 3809. https://doi.org/10.3390/rs14153809.
Liu, B., Huang, H., Su, Y., Chen, S., Li, Z., Chen, E., Tian, X., 2022b. Tree species classification using ground-based LiDAR data by various point cloud deep learning methods. Rem. Sens. 14, 5733. https://doi.org/10.3390/rs14225733.
Liu, J., Chen, J.M., Cihlar, J., Chen, W., 2002. Net primary productivity mapped for Canada at 1-km resolution. Global Ecol. Biogeogr. 11, 115–129. https://doi.org/10.1046/j.1466-822X.2002.00278.x.
Loshchilov, I., Hutter, F., 2019. Decoupled Weight Decay Regularization. https://doi.org/10.48550/arXiv.1711.05101.
Loshchilov, I., Hutter, F., 2017. SGDR: Stochastic Gradient Descent with Warm Restarts. https://doi.org/10.48550/arXiv.1608.03983.
Luo, S., Wang, C., Xi, X., Pan, F., Peng, D., Zou, J., Nie, S., Qin, H., 2017. Fusion of airborne LiDAR data and hyperspectral imagery for aboveground and belowground forest biomass estimation. Ecol. Indicat. 73, 378–387. https://doi.org/10.1016/j.ecolind.2016.10.001.
Ma, L., Liu, Y., Zhang, X., Ye, Y., Yin, G., Johnson, B.A., 2019. Deep learning in remote sensing applications: a meta-analysis and review. ISPRS J. Photogrammetry Remote Sens. 152, 166–177. https://doi.org/10.1016/j.isprsjprs.2019.04.015.
Magalhães, T.M., Seifert, T., 2015. Tree component biomass expansion factors and root-to-shoot ratio of Lebombo ironwood: measurement uncertainty. Carbon Bal. Manag. 10, 9. https://doi.org/10.1186/s13021-015-0019-4.
Mahoney, M.J., Johnson, L.K., Bevilacqua, E., Beier, C.M., 2022. Filtering ground noise from LiDAR returns produces inferior models of forest aboveground biomass in heterogenous landscapes. GIScience Remote Sens. 59, 1266–1280. https://doi.org/10.1080/15481603.2022.2103069.

Maltman, J.C., Hermosilla, T., Wulder, M.A., Coops, N.C., White, J.C., 2023. Estimating and mapping forest age across Canada's forested ecosystems. Rem. Sens. Environ. 290, 113529 https://doi.org/10.1016/j.rse.2023.113529.
Martin, G., 2003. Management of New Brunswick's Crown Forest. Department of Natural Resources.
Mäyrä, J., Keski-Saari, S., Kivinen, S., Tanhuanpää, T., Hurskainen, P., Kullberg, P., Poikolainen, L., Viinikka, A., Tuominen, S., Kumpula, T., Vihervaara, P., 2021. Tree species classification from airborne hyperspectral and LiDAR data using 3D convolutional neural networks. Rem. Sens. Environ. 256, 112322 https://doi.org/10.1016/j.rse.2021.112322.
McRoberts, R.E., Næsset, E., Gobakken, T., Bollandsås, O.M., 2015. Indirect and direct estimation of forest biomass change using forest inventory and airborne laser scanning data. Rem. Sens. Environ. 164, 36–42. https://doi.org/10.1016/j.rse.2015.02.018.
Momo Takoudjou, S., Ploton, P., Sonké, B., Hackenberg, J., Griffon, S., de Coligny, F., Kamdem, N.G., Libalah, M., Mofack, G.I., Le Moguédec, G., Pélissier, R., Barbier, N., 2018. Using terrestrial laser scanning data to estimate large tropical trees biomass and calibrate allometric models: a comparison with traditional destructive approach. Methods Ecol. Evol. 9, 905–916. https://doi.org/10.1111/2041-210X.12933.
Narine, L.L., Popescu, S.C., Malambo, L., 2019. Synergy of ICESat-2 and Landsat for mapping forest aboveground biomass with deep learning. Rem. Sens. 11, 1503. https://doi.org/10.3390/rs11121503.
Natural Resources Canada, 2022. CBM-CFS3 [WWW Document]. URL. https://naturalresources.canada.ca/climate-change/climate-change-impacts-forests/carbon-accounting/carbon-budget-model/13107. accessed 7.10.23.
Navarrete-Poyatos, M.A., Navarro-Cerrillo, R.M., Lara-Gómez, M.A., Duque-Lazo, J., Varo, M.d.l.A., Palacios Rodriguez, G., 2019. Assessment of the carbon stock in pine plantations in southern Spain through ALS data and K-nearest neighbor algorithm based models. Geosciences 9, 442. https://doi.org/10.3390/geosciences9100442.
Nguyen, T.-A., Kellenberger, B., Tuia, D., 2022. Mapping forest in the Swiss Alps treeline ecotone with explainable deep learning. Rem. Sens. Environ. 281, 113217 https://doi.org/10.1016/j.rse.2022.113217.
Nguyen, T.H., Jones, S., Soto-Berelov, M., Haywood, A., Hislop, S., 2018. A comparison of imputation approaches for estimating forest biomass using Landsat time-series and inventory data. Rem. Sens. 10, 1825. https://doi.org/10.3390/rs10111825.
Oehmcke, S., Li, L., Revenga, J.C., Nord-Larsen, T., Trepekli, K., Gieseke, F., Igel, C., 2022. Deep learning based 3D point cloud regression for estimating forest biomass. In: Proceedings of the 30th International Conference on Advances in Geographic Information Systems, SIGSPATIAL '22. Association for Computing Machinery, New York, NY, USA, pp. 1–4. https://doi.org/10.1145/3557915.3561471.
Oubara, A., Wu, F., Amamra, A., Yang, G., 2022. Survey on remote sensing data augmentation: advances, challenges, and future perspectives. In: Senouci, M.R., Boulahia, S.Y., Benatia, M.A. (Eds.), Advances in Computing Systems and Applications, Lecture Notes in Networks and Systems. Springer International Publishing, Cham, pp. 95–104. https://doi.org/10.1007/978-3-031-12097-8_9.
Pan, Y., Birdsey, R.A., Fang, J., Houghton, R., Kauppi, P.E., Kurz, W.A., Phillips, O.L., Shvidenko, A., Lewis, S.L., Canadell, J.G., Ciais, P., Jackson, R.B., Pacala, S.W., McGuire, A.D., Piao, S., Rautiainen, A., Sitch, S., Hayes, D., 2011. A large and persistent carbon sink in the world's forests. Science 333, 988–993. https://doi.org/10.1126/science.1201609.
Parresol, B.R., 2001. Additivity of nonlinear biomass equations. Can. J. For. Res. 31, 865–878. https://doi.org/10.1139/x00-202.
Paszke, A., Gross, S., Massa, F., Lerer, A., Bradbury, J., Chanan, G., Killeen, T., Lin, Z., Gimelshein, N., Antiga, L., Desmaison, A., Kopf, A., Yang, E., DeVito, Z., Raison, M., Tejani, A., Chilamkurthy, S., Steiner, B., Fang, L., Bai, J., Chintala, S., Wallach, H., Larochelle, H., Beygelzimer, A., d'Alché-Buc, F., Fox, E., Garnett, R., 2019. PyTorch: an imperative style, high-performance deep learning library. Adv. Neural Inf. Process. Syst. 32.
Pedregosa, F., Varoquaux, G., Gramfort, A., Michel, V., Thirion, B., Grisel, O., Blondel, M., Prettenhofer, P., Weiss, R., Dubourg, V., Vanderplas, J., Passos, A., Cournapeau, D., Brucher, M., Perrot, M., Duchesnay, É., 2011. Scikit-learn: machine learning in Python. J. Mach. Learn. Res. 12, 2825–2830.
Peter, B., Niquidet, K., 2016. Estimates of residual fibre supply and the impacts of new bioenergy capacity from a forest sector transportation model of the Canadian Prairie Provinces. For. Pol. Econ. 69, 62–72. https://doi.org/10.1016/j.forpol.2016.05.003.
Popescu, S.C., 2007. Estimating biomass of individual pine trees using airborne lidar. Biomass and Bioenergy, Multiple benefits from sustainable bioenergy systems 31, 646–655. https://doi.org/10.1016/j.biombioe.2007.06.022.
Qi, C.R., Su, H., Mo, K., Guibas, L.J., 2017a. PointNet: Deep Learning on Point Sets for 3D Classification and Segmentation arXiv:1612.00593 [cs].
Qi, C.R., Yi, L., Su, H., Guibas, L.J., 2017b. Pointnet++: deep hierarchical feature learning on point sets in a metric space. Adv. Neural Inf. Process. Syst. 30 https://doi.org/10.48550/arXiv.1706.02413.
R Core Team, 2023. R: A Language and Environment for Statistical Computing. R Foundation for Statistical Computing, Vienna, Austria.
Reichstein, M., Carvalhais, N., 2019. Aspects of forest biomass in the earth system: its role and major unknowns. Surv. Geophys. 40, 693–707. https://doi.org/10.1007/s10712-019-09551-x.
Rex, F.E., Silva, C.A., Dalla Corte, A.P., Klauberg, C., Mohan, M., Cardil, A., Silva, V.S. da, Almeida, D.R.A. de, Garcia, M., Broadbent, E.N., Valbuena, R., Stoddart, J., Merrick, T., Hudak, A.T., 2020. Comparison of statistical modelling approaches for estimating tropical forest aboveground biomass stock and reporting their changes in low-intensity logging areas using multi-temporal LiDAR data. Rem. Sens. 12, 1498. https://doi.org/10.3390/rs12091498.
Ribeiro, M.T., Singh, S., Guestrin, C., 2016. "Why should I trust you?" Explaining the predictions of any classifier. In: Presented at the Proceedings of the 22nd ACM SIGKDD International Conference on Knowledge Discovery and Data Mining, pp. 1135–1144.
Rodríguez-Soalleiro, R., Eimil-Fraga, C., Gómez-García, E., García-Villabrille, J.D., Rojo-Alboreca, A., Muñoz, F., Oliveira, N., Sixto, H., Pérez-Cruzado, C., 2018. Exploring the factors affecting carbon and nutrient concentrations in tree biomass components in natural forests, forest plantations and short rotation forestry. Forest Ecosystems 5, 35. https://doi.org/10.1186/s40663-018-0154-y.
Roussel, J.-R., Auty, D., Coops, N.C., Tompalski, P., Goodbody, T.R.H., Meador, A.S., Bourdon, J.-F., de Boissieu, F., Achim, A., 2020. lidR: an R package for analysis of Airborne Laser Scanning (ALS) data. Rem. Sens. Environ. 251, 112061 https://doi.org/10.1016/j.rse.2020.112061.
Rusu, R.B., Cousins, S., 2011. 3d is here: point cloud library (pcl). In: Presented at the 2011 IEEE International Conference on Robotics and Automation. IEEE, pp. 1–4.
Sanquetta, C.R., Behling, A., Corte, A.P.D., Péllico Netto, S., Schikowski, A.B., do Amaral, M.K., 2015. Simultaneous estimation as alternative to independent modeling of tree biomass. Ann. For. Sci. 72, 1099–1112. https://doi.org/10.1007/s13595-015-0497-2.
Schmohl, S., Sörgel, U., 2019. Submanifold sparse convolutional networks for semantic segmentation of large-scale ALS point clouds. In: ISPRS Annals of the Photogrammetry, Remote Sensing and Spatial Information Sciences. Presented at the ISPRS Geospatial Week 2019, IV-2/W5. Copernicus GmbH, Enschede, The Netherlands, pp. 77–84. https://doi.org/10.5194/isprs-annals-IV-2-W5-77-2019, 10–14 June 2019.
Seely, H., 2023. Harryseely/Biomass-DL: v1.0.0. https://doi.org/10.5281/zenodo.10086250.
Shendryk, Y., 2022. Fusing GEDI with earth observation data for large area aboveground biomass mapping. Int. J. Appl. Earth Obs. Geoinf. 115, 103108 https://doi.org/10.1016/j.jag.2022.103108.
Shrikumar, A., Greenside, P., Kundaje, A., 2017. Learning important features through propagating activation differences. In: Proceedings of the 34th International Conference on Machine Learning. Presented at the International Conference on Machine Learning. PMLR, pp. 3145–3153.
Sun, K., Xiao, B., Liu, D., Wang, J., 2019. Deep high-resolution representation learning for human pose estimation. In: Presented at the Proceedings of the IEEE/CVF Conference on Computer Vision and Pattern Recognition, pp. 5693–5703.
Tan, H., Kotthaus, H., 2023. Explainability-aware one point attack for point cloud neural networks. In: 2023 IEEE/CVF Winter Conference on Applications of Computer Vision (WACV). Presented at the 2023 IEEE/CVF Winter Conference on Applications of Computer Vision. WACV, pp. 4570–4579. https://doi.org/10.1109/WACV56688.2023.00456.
Tan, H., Kotthaus, H., 2022. Surrogate model-based explainability methods for point cloud NNs. In: Presented at the Proceedings of the IEEE/CVF Winter Conference on Applications of Computer Vision, pp. 2239–2248.
Tompalski, P., Roussel, J.-R., Woods, M., Hambrecht, L., 2023. lidRmetrics [WWW Document]. URL. https://github.com/ptompalski/lidRmetrics. accessed 7.13.23.
Tsitsi, B., 2016. Remote sensing of aboveground forest biomass: a review. Trop. Ecol. 57, 125–132.
Turgeon-Pelchat, M., Foucher, S., Bouroubi, Y., 2021. Deep learning-based classification of large-scale airborne LiDAR point cloud. Can. J. Rem. Sens. 47, 381–395. https://doi.org/10.1080/07038992.2021.1927687.
Turrado Fernández, S., Paredes Sánchez, J.P., Gutiérrez Trashorras, A.J., 2016. Analysis of forest residual biomass potential for bioenergy production in Spain. Clean Technol. Environ. Policy 18, 209–218. https://doi.org/10.1007/s10098-015-1008-8.
Ung, C.-H., Bernier, P., Guo, X.-J., 2008. Canadian national biomass equations: new parameter estimates that include British Columbia data. Can. J. For. Res. 38, 1123–1132. https://doi.org/10.1139/X07-224.
Vorster, A.G., Evangelista, P.H., Stovall, A.E.L., Ex, S., 2020. Variability and uncertainty in forest biomass estimates from the tree to landscape scale: the role of allometric equations. Carbon Bal. Manag. 15, 8. https://doi.org/10.1186/s13021-020-00143-6.
Wang, P.-S., 2023. O-CNN [WWW Document]. URL. https://github.com/octree-nn/ocnn-pytorch. accessed 5.3.23.
Wang, P.-S., Liu, Y., Guo, Y.-X., Sun, C.-Y., Tong, X., 2017. O-CNN: octree-based convolutional neural networks for 3D shape analysis. ACM Trans. Graph. 36 (72), 1–72. https://doi.org/10.1145/3072959.3073608, 11.
Wang, P.-S., Liu, Y., Tong, X., 2020. Deep Octree-Based CNNs with Output-Guided Skip Connections for 3D Shape and Scene Completion. https://doi.org/10.48550/arXiv.2006.03762.
Wang, P.-S., Sun, C.-Y., Liu, Y., Tong, X., 2018. Adaptive O-CNN: a patch-based deep representation of 3D shapes. ACM Trans. Graph. 37, 1–11. https://doi.org/10.1145/3272127.3275050.
Wang, P.-S., Yang, Y.-Q., Zou, Q.-F., Wu, Z., Liu, Y., Tong, X., 2021. Unsupervised 3D Learning for Shape Analysis via Multiresolution Instance Discrimination. https://doi.org/10.48550/arXiv.2008.01068.
Wang, Y., Sun, Y., Liu, Z., Sarma, S.E., Bronstein, M.M., Solomon, J.M., 2019. Dynamic Graph CNN for Learning on Point Clouds.
Weinstein, B.G., Marconi, S., Bohlman, S.A., Zare, A., White, E.P., 2020. Cross-site learning in deep learning RGB tree crown detection. Ecol. Inf. 56, 101061 https://doi.org/10.1016/j.ecoinf.2020.101061.
White, J.C., Coops, N.C., Wulder, M.A., Vastaranta, M., Hilker, T., Tompalski, P., 2016. Remote sensing technologies for enhancing forest inventories: a review. Can. J. Rem. Sens. 42, 619–641. https://doi.org/10.1080/07038992.2016.1207484.
White, J.C., Stepper, C., Tompalski, P., Coops, N.C., Wulder, M.A., 2015. Comparing ALS and image-based point cloud metrics and modelled forest inventory attributes in a complex coastal forest environment. Forests 6, 3704–3732. https://doi.org/10.3390/f6103704.

Widagdo, F.R.A., Li, F., Zhang, L., Dong, L., 2020. Aggregated biomass model systems and carbon concentration variations for tree carbon quantification of natural Mongolian oak in northeast China. Forests 11, 397. https://doi.org/10.3390/f11040397.

Winiwarter, L., 2023. pyForMetrix [WWW Document]. Zenodo. URL, 10.5281/zenodo.8183806.

Winiwarter, L., Mandlburger, G., Schmohl, S., Pfeifer, N., 2019. Classification of ALS point clouds using end-to-end deep learning. PFG–journal of photogrammetry, remote sensing and geoinformation science 87, 75–90.

Woods, M., Lim, K., Treitz, P., 2008. Predicting forest stand variables from LiDAR data in the great lakes - st. Lawrence forest of ontario. For. Chron. 84, 827–839. https://doi.org/10.5558/tfc84827-6.

Xu, D., Wang, H., Xu, W., Luan, Z., Xu, X., 2021. LiDAR applications to estimate forest biomass at individual tree scale: opportunities, challenges and future perspectives. Forests 12, 550. https://doi.org/10.3390/f12050550.

Xu, Y., Gong, J., Huang, X., Hu, X., Li, J., Li, Q., Peng, M., 2022. Luojia-HSSR: a high spatial-spectral resolution remote sensing dataset for land-cover classification with a new 3D-HRNet. Geo-Spatial Inf. Sci. 1–13.

Xu, Z., Li, W., Li, Y., Shen, X., Ruan, H., 2019. Estimation of secondary forest parameters by integrating image and point cloud-based metrics acquired from unmanned aerial vehicle. JARS 14, 022204. https://doi.org/10.1117/1.JRS.14.022204.

Zelazny, V.F., Martin, G., Toner, M., Gorman, M., Colpitts, M., Veen, H., Godin, B., McInnis, B., Steeves, C., Roberts, M., 2007. Our Landscape Heritage: the Story of Ecological Land Classification in New Brunswick. New Brunswick Department of Natural Resources, Hugh John Fleming Forestry Centre, Fredericton, NB E3C 2G6, Canada.

Zeng, P., Shi, J., Huang, J., Zhang, Y., Zhang, W., 2022. Component forest above ground biomass estimation using lidar and sardata. In: IGARSS 2022 - 2022 IEEE International Geoscience and Remote Sensing Symposium. Presented at the IGARSS 2022 - 2022 IEEE International Geoscience and Remote Sensing Symposium, pp. 6395–6398. https://doi.org/10.1109/IGARSS46834.2022.9883852.

Zhang, J., Lin, S., Ding, L., Bruzzone, L., 2020. Multi-scale context aggregation for semantic segmentation of remote sensing images. Rem. Sens. 12, 701.

Zhang, L., Shao, Z., Liu, J., Cheng, Q., 2019. Deep learning based retrieval of forest aboveground biomass from combined LiDAR and Landsat 8 data. Rem. Sens. 11, 1459. https://doi.org/10.3390/rs11121459.

Zhang, Li, Luo, Y., Yu, G., Zhang, Leiming, 2010. Estimated carbon residence times in three forest ecosystems of eastern China: applications of probabilistic inversion. J. Geophys. Res.: Biogeosciences 115. https://doi.org/10.1029/2009JG001004.

Zhang, Liangpei, Zhang, Lefei, Du, B., 2016. Deep learning for remote sensing data: a technical tutorial on the state of the art. IEEE Geoscience and Remote Sensing Magazine 4, 22–40. https://doi.org/10.1109/MGRS.2016.2540798.

Zhang, Y., Ma, J., Liang, S., Li, X., Liu, J., 2022. A stacking ensemble algorithm for improving the biases of forest aboveground biomass estimations from multiple remotely sensed datasets. GIScience Remote Sens. 59, 234–249. https://doi.org/10.1080/15481603.2021.2023842.

Zhao, D., Westfall, J., Coulston, J.W., Lynch, T.B., Bullock, B.P., Montes, C.R., 2019. Additive biomass equations for slash pine trees: comparing three modeling approaches. Can. J. For. Res. 49, 27–40. https://doi.org/10.1139/cjfr-2018-0246.

Zhao, H., Jiang, L., Jia, J., Torr, P.H.S., Koltun, V., 2021. Point transformer. In: Presented at the Proceedings of the IEEE/CVF International Conference on Computer Vision, pp. 16259–16268.

Zhao, K., Popescu, S., Nelson, R., 2009. Lidar remote sensing of forest biomass: a scale-invariant estimation approach using airborne lasers. Rem. Sens. Environ. 113, 182–196. https://doi.org/10.1016/j.rse.2008.09.009.

Zhou, K., Cao, L., Liu, H., Zhang, Z., Wang, G., Cao, F., 2022. Estimation of volume resources for planted forests using an advanced LiDAR and hyperspectral remote sensing. Resour. Conserv. Recycl. 185, 106485. https://doi.org/10.1016/j.resconrec.2022.106485.

Zhou, B., Khosla, A., Lapedriza, A., Oliva, A., Torralba, A., 2016. Learning deep features for discriminative localization. In: Presented at the Proceedings of the IEEE Conference on Computer Vision and Pattern Recognition, pp. 2921–2929.

Zhou, Q.-Y., Park, J., Koltun, V., 2018. Open3D: A Modern Library for 3D Data Processing arXiv preprint arXiv:1801.09847.

Zolkos, S.G., Goetz, S.J., Dubayah, R., 2013. A meta-analysis of terrestrial aboveground biomass estimation using lidar remote sensing. Rem. Sens. Environ. 128, 289–298. https://doi.org/10.1016/j.rse.2012.10.017.